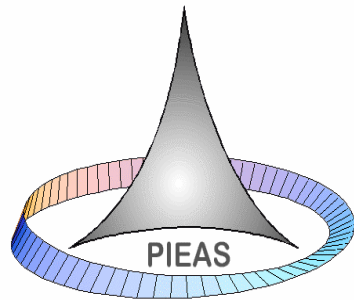# Iris Recognition Based
Biometric Security System

PIEAS

By

Azad Ali

Department of Electrical Engineering,

Pakistan Institute of Engineering and Applied Sciences,

Nilore, Islamabad, Pakistan

AUGUST, 2005

CERTIFICATE OF APPROVAL

It is certified that the work contained in this thesis entitled

"Iris Recognition Based Biometric Security System"

was carried out by **Azad Ali** under my supervision and that in my opinion, it is fully adequate, in scope and quality, for the degree of **M.Sc. Systems Engineering**.

Approved by:

Supervisor: Nadeem Qaiser

Signature: _____

August 2005.

Tables of Contents

List of Figures

List of Abbreviation

HT	Hough Transform
CHT	Circular Hough Transform
CWT	Continuous Wavelet Transform
DWT	Discrete Wavelet Transform
FAR	False Acceptance Rate
FRR	False Rejection Rate
EER	Equal Error Rate

Abstract

A biometric system provides automatic identification of an individual through physiological features or behavioral traits. Iris recognition is regarded as the most reliable and accurate biometric identification system available. An in-depth study of the problem has been carried out and a successful implementation has been made in Matlab.

The study of the problem revealed it to be a two stage problem. In the first stage it's a computer vision problem that addresses the issues of the segmentation of the useful area of the eye, detection of the noise and occlusion. The second stage of the problem is a texture analysis problem. In this the features from the segmented image are extracted.

The segmentation stage is performed using circular Hough transform (CHT). Various optimization techniques are used to reduce the computation time and resources required by CHT. Normalization is performed to convert the donut shaped iris into a strip to account for imaging inconsistencies. After trying out different techniques for locating the occlusion of the eyes it was finally figured out that it is best to locate the occlusion after normalization. So proposed occlusion detection algorithm performs reliably and better than the other techniques cited in literature.

To extract the features a number of filtering techniques were used and it was figured out that the best techniques in the case of iris textures is Wavelets, as it analyzes the texture at different scales hence locally capturing the different patterns occurring at different scales. The wavelet coefficients at different scales were chosen, and then quantized to form a binary code that we call as iris template.

The Hamming distance is employed for classification of iris templates, and two templates are found to match if a test of statistical independence is failed. The developed system proved to be stable against camera defocusing, head tilting and to some extent to the noise. The performance of the system was tested on two sets of data and found out to be reliable, with 93% of proper segmentation results and 87.28% of the proper classification. The failure of the classification was mostly due to over occluded eye or too much noise of eyelashes.

Keywords: iris recognition, biometric identification, pattern recognition, circular Hough transform, automatic segmentation, wavelets.

Chapter 1

INTRODUCTION

The iris is a protected internal organ of the eye, located behind the cornea and the aqueous humour, but in front of the lens. A visible property of the iris and the fingerprint is the random morphogenesis of their minutiae. The phenotypic expression even of two irises with the same genetic genotype (as in identical twins, or the pair possessed by one individual) have uncorrelated minutiae. The iris texture has no genetic penetrance in the expression and is chaotic. In these respects the uniqueness of every iris parallels the uniqueness of every fingerprint, common genotype or not. But the iris enjoys further practical advantages over fingerprint [2]. Hence it is widely being used now for the biometric security systems.

1.1 The Human Iris

Human eye is divided into two chambers. The first one is the anterior chamber and the second one is the posterior chamber, which are separated by iris and lens. The anatomy of the human eye is shown in Fig. 1.1.

FIGURE 1-1 HUMAN EYE
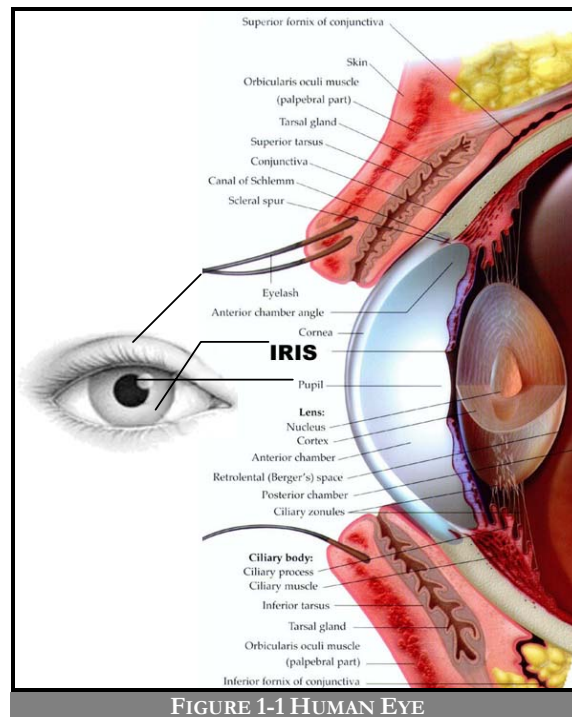
The human iris begins to form during the third month of gestation. The structure is complete by the eighth month of gestation, but pigmentation continues into the first year after birth. The iris grows from the ciliary body and its colour is given by the amount of pigment and by the density of the iris tissue that means from blue to black. The most important function of the iris is controlling the size of the pupil. Illumination, which enters the pupil and falls on the retina of the eye, is controlled by muscles in the iris.

They regulate the size of the pupil and this is what permits the iris to control the amount of light entering the pupil. The change in the size results from involuntary reflexes and is not under conscious control. The tissue of the iris is soft and loosely woven and it is called STROMA.

Section through the human iris is shown in Fig. 1.2. In this figure, we can see the layers of the human iris. The layers of the iris have both ectodermal and mesodermal embryological origin. The visible one is the anterior layer, which bears the gaily-colored relief and it is very lightly pigmented due to genetically determined density of melanin pigment granules. The invisible one is the posterior layer, which is very darkly pigmented, contrary to the anterior layer. The surface of this layer is finely radiantly and concentrically furrowed with dark brown color. Muscles and the vascularized stroma are found between these layers from back to front. Pigment frill is the boundary between the pupil and the human iris. It is a visible section of the posterior layer and looks like a curling edge of the pupil. The whole anterior layer consists of the pupillary area and the ciliary area and their boundary is called collarette. The ciliary area is divided into the inner area, which is relatively smooth and bears radial furrows, the middle area, heavily furrowed in all directions and with pigment piles on the ridges, and the outer marginal area bearing numerous periphery crypts.
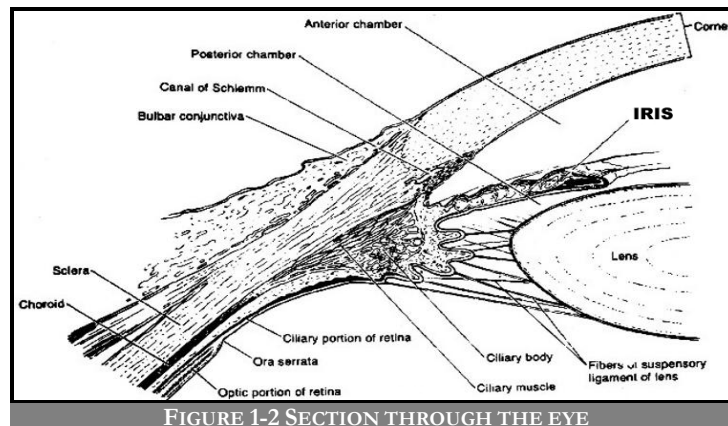
FIGURE 1-2 SECTION THROUGH THE EYE

1.2 Features of the Human Iris

Now some of the visible features of the human iris will be described, which are important to identify a person, especially pigment related features, features controlling the size of the pupil, visible rare anomalies, pupil, pigment frill and collarette.

Among the pigment related features belong the crypts and the pigment spots, which are shown in Fig. 1.3. The crypts, in the figure shown as number 3, are the areas in which the iris is relatively thin. They have very dark colour due to dark colour of the posterior layer. They appear near the collarette, or on the periphery of the iris. They

look likesharply demarcated excavations. The pigment spots, in the figure shown as number 4, are random concentrations of pigment cells in the visible surface of the iris and generally appear in the ciliary area. They are known as moles and freckles with nearly black colour.

FIGURE 1-3 PIGMENT RELATED FEATURE (1. PUPIL, 2. IRIS, 3- CRYPTS, 4. PIGMENT SPOTS, 5. RADIAL FURROWS, 6. CONVENTRIC FURROWS, 7. COLLARETTE, 8. PIGMENT FRILL)
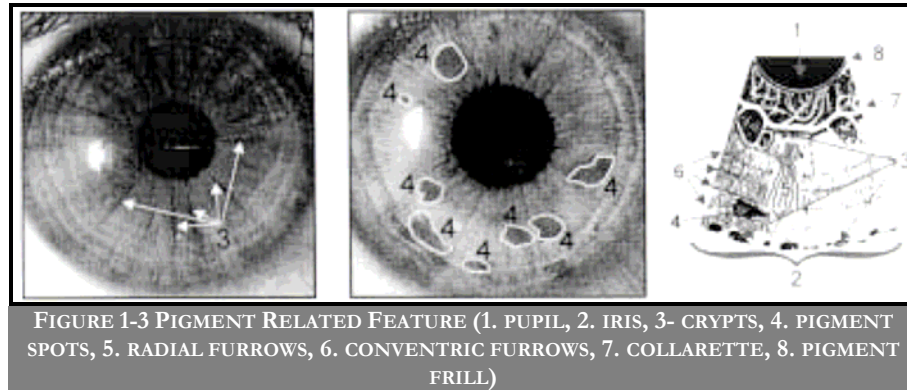
Features controlling the size of the pupil are radial and concentric furrows. They are called contraction furrows and control the size of the pupil. Extending radially, number 5 in Fig. 5, in relation to the center of the pupil are radial furrows. The typical radial furrows may begin near the pupil and extend through the collarette. The radial furrows are creased in the anterior layer of the iris, from which loose tissue may bulge outward and this is what permits the iris to change the size of the pupil. The concentric furrows, number 6 in Fig. 1.4, are generally circular and concentric with the pupil. They typically appear in the ciliary area, near the periphery of the iris and permit to bulge the loose tissue outward in different direction than the radial furrows. Collarette, mentioned brie- y above, is the boundary between the ciliary area and the pupillary area. It is a sinuous line shown as number 7 in Fig. 1.5, which forms an elevated ridge running parallel with the margin of the pupil. The collarette is the thickest part of the human iris.

FIGURE 1-4 FEATURES CONTROLLING THE SIZE OF THE PUPIL (1. PUPIL, 2- IRIS, 3. CRYPTS, 4. PIGMENT SPOTS, 5. RADIAL FURROWS, 6. CONCENTRIC FURROWS, 7. COLLARETTE, 8. PIGMENT FRILL)
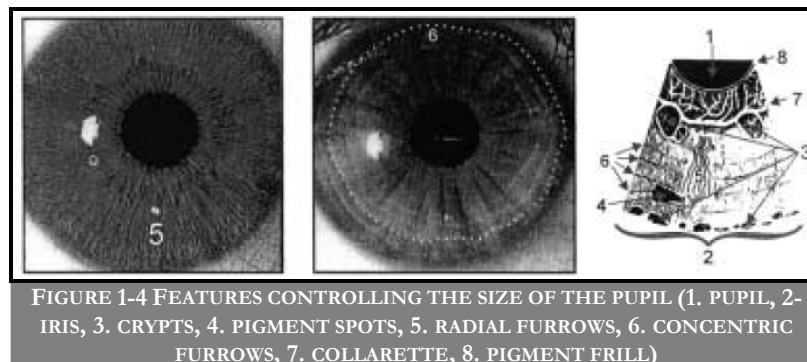
Finally, the most striking visible feature of the eye is typically the pupil. The pupil is shown as 1 in Fig. 1.3, 1.4, 1.5, it may not be exactly circular in shape and its deviation from the circle is a visible characteristics. Centers of the iris and the pupil are different and they can differ from each other of about 20 %. There is a protruding portion of the posterior layer of the iris at the margin of the pupil, the pigment frill number 8 in Fig. 1.3, 1.4, 1.5, which was described above.

FIGURE 1-5 COLLARETTE (1. PUPIL, 2. IRIS, 3. CRUPTS, 4. PIGMENT SPOTS, 5. RADIAL FURROWS, 6. CONCENTRIC FURROWS, 7. COLLARETTE, 8. PIGMENT FRILL)
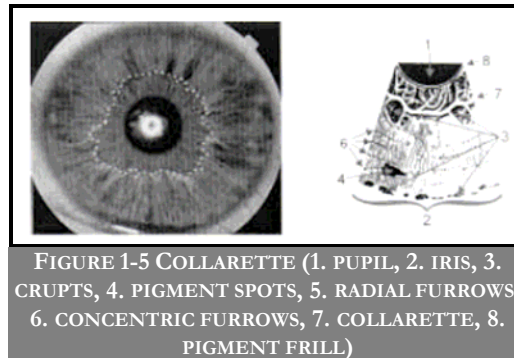
1.3 Why Iris?

The most important features, which make the iris recognition the most attractive as compared to other biometric techniques, are as follows

- Highly protected, internal organ of the eye
- Highly accurate
- Externally visible, from arm's length distance
- Random pattern of great complexity and
- Uniqueness
- Pattern is epigenetic (not genetically determined)
- Stable through life
- The impossibility of surgically modifying it without unacceptable risk to vision
- its physiological response to light, which provides a natural test against artifice
- its intrinsic polar geometry, which imparts a natural coordinate system and an origin of coordinates
- Encoding and matching are reliable and fast
- The printing process adds a characteristic signature of periodicity to the 2D Fourier power spectrum

Iris recognition, compared to other biometrics technologies, has the lowest FRR and FAR. As the following graph shows, iris recognition is constantly above 1% in the FRR and constantly at 0.00001% at the FAR [3].

FIGURE 1-6 PERFORMANCE COMPARISON FOR SEVERAL TYPES OF BIOMETRIC TECHNOLOGIES. IRIS IS ON THE VERTICAL AXIS[UK NATIONAL PHYSICAL LABORATORY 2001]
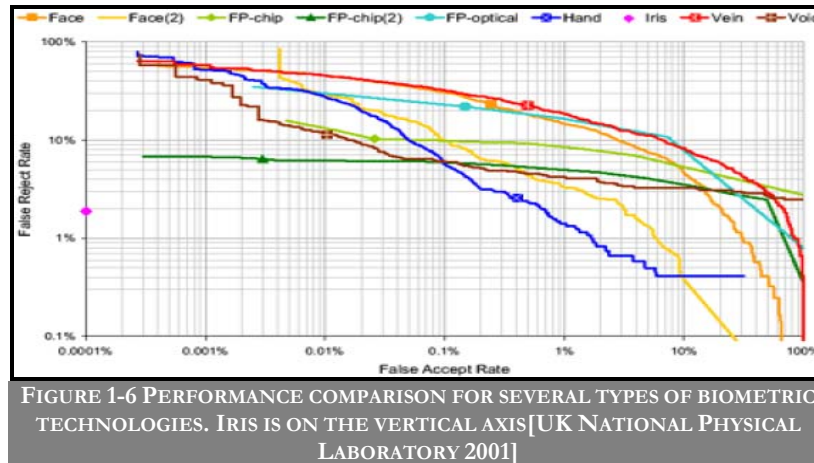
1.4 Recognition of Iris

The main steps in the recognition of iris are as follows:

• Segmentation

• Normalization

• Feature Encoding

• Feature Matching

Chapter 2

Iris Segmentation and Normalization

The first stage of iris recognition is to isolate the actual iris region in a digital eye image. The iris region can be approximated by two circles, one for the iris/sclera boundary and another, interior to the first, for the iris/pupil boundary. The eyelids and eyelashes normally occlude the upper and lower parts of the iris region. A technique is required to isolate and exclude these artifacts as well as locating the circular iris region.

The success of segmentation depends on the imaging quality of eye images. Persons with darkly pigmented irises will present very low contrast between the pupil and iris region if imaged under natural light, making segmentation more difficult. The segmentation stage is critical to the success of an iris recognition system, since data that is falsely represented as iris pattern data will corrupt the biometric templates generated, resulting in poor recognition rates.

2.1 Segmentation of Iris

The main steps involved in the segmentation are

- Preprocessing
- Hough Transform

2.1.1 Preprocessing

Before we go any further we need to perform a little preprocessing. As for the segmentation stage we need an edge binary image. For this Canny Edge detector is selected, as it yields the optimal edge results. Moreover it has very much flexible parameter like the Gaussian spread and the edge connectivity, so that we can easily remove noise and keep the points well connected. In some databases like the UBIRIS, gamma correction is a curtail stage, not employing a contrast correction algorithm may result into failure of segmentation stage and hence consequently the recognition.

FIGURE 2-1 EDGE DETECTED IMAGE

2.1.2 Hough transform

The Hough transform is a standard computer vision algorithm that can be used to determine the parameters of simple geometric objects, such as lines and circles, present in an image.

To use the Hough transform, we need a way to characterize a line. One representation of a line is the slope-intercept form

$$y = mx + c \qquad\qquad \text{Eq: 2-1}$$

where '*m*' is the slope of the line and '*c*' is the y-intercept. Given this characterization of a line, we can then iterate through any number of lines that pass through any given points. By iterating through fixed values of '*m*', we can solve for '*b*' by

$$c = y - mx \qquad\qquad \text{Eq: 2-2}$$

However, this method is not very stable. As lines get more and more vertical, the magnitudes of and grow towards infinity. A more useful representation of a line is its normal form.

$$x\cos\theta + y\sin\theta = \rho$$

<div align="right">Eq: 2-3</div>

This equation specifies a line passing through (x, y) that is perpendicular to the line drawn from the origin to (θ, ρ) in polar space. For each point (x, y) on a line, and (θ, ρ) are constant.

Now, for any given point, we can obtain lines passing through that point by solving for ρ and θ. By iterating through possible angles for θ, we can solve for ρ by using above equation directly. This method proves to be more effective than the first one, as it is numerically stable for matching lines of any angle.

2.1.3 Circular Hough Transform

The Hough transform can be used for representing other objects besides lines. For instance, a circle can be parameterized as

$$(x-a)^2 + (y-b)^2 = r^2$$

<div align="right">Eq: 2-4</div>

Here, (a, b) is the coordinate of the center of the circle that passes through (x, y), and 'r' is its radius. Since there are three parameters for this equation, it follows that the Hough transform will be a three-dimensional. Therefore circles require more computation to find than lines.

To carryout the Hough transform we keep on picking the edge pixels and project these points in the Hough space i.e. vote the points in the image to be the center of the circle. In other words we make a circle around each edge point and when these are projected at the right radius these circles pass through the same center resulting in the maximum voting for that pixel to be the center of the circle.

But this form of the equation of the circle given by eq. 2.4 is rather computationally expensive, as we have to keep a very high resolution of the independent variable 'x' to extract each point in the image domain. Hence in the implementation the polar form given by the following set of equations is used

$$x = r\cos\theta + a$$
$$y = r\sin\theta + b$$

<div align="right">Eq: 2-5</div>

where 'r' is the radius of the circle, (a, b) is the center of the circle and 'θ' is the angle of rotation.

FIGURE 2-2 INPUT IMAGE TO HT

FIGURE 2-3 TRANSFORM WHEN RADIUS IS NOT APPROPRIATE

FIGURE 2-4 TRANSFORM AT THE EXACT RADIUS OF THE CIRCLE
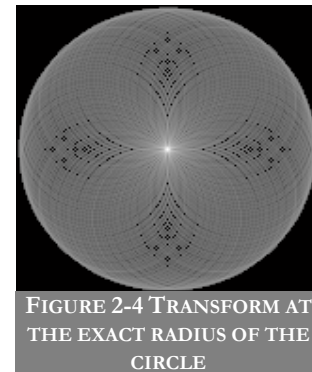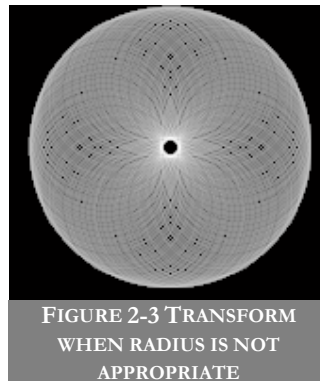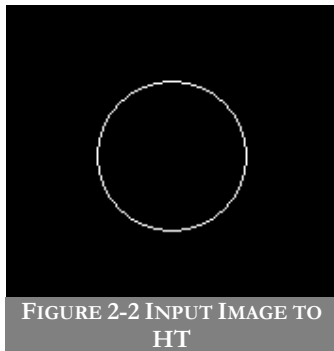
2.1.4 Detection of Pupil and Iris

Circular Hough transform (CHT) has been employed for the detection of the pupil-iris boundary and the iris-sclera boundary. Results of applying the Hough transform are shown below

FIGURE 2-5 INPUT IRIS IMAGE

FIGURE 2-6 HOUGH TRANSFORM OF THE INPUT

FIGURE 2-7 GAMMA CORRECTION OF HT TO SHOW DETAILS

FIGURE 2-8 MESH OF HOUGH TRANSFORM SHOWING PEAK FOR THE PUPIL CENTER
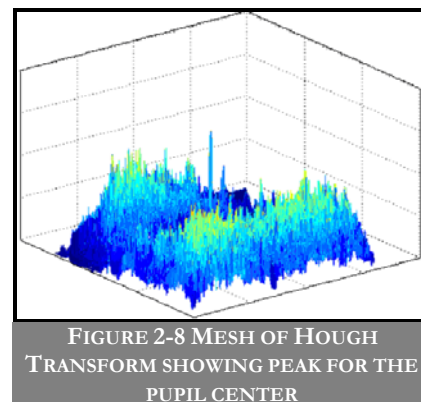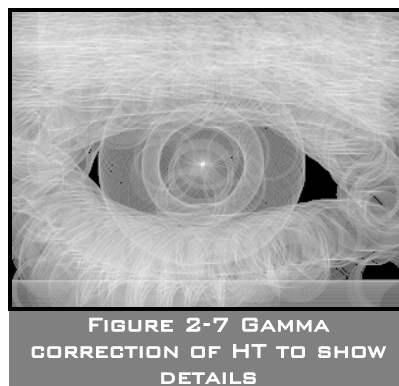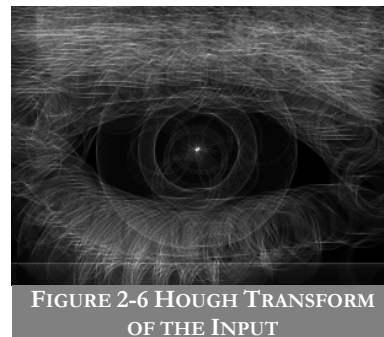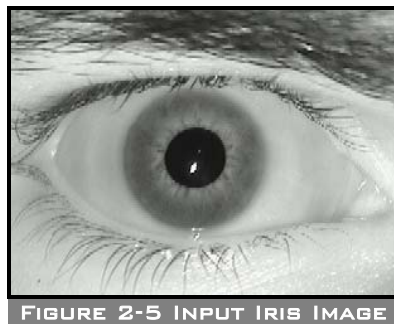
The pictures above show the Hough transform result when the radius is equal to the radius of the pupil. The picture above and the mesh clearly show the centre of the circle (pupil) with the maximum voting, hence the largest peek in the mesh and the

brightest spot in the picture. The gamma corrected image illustrates the portion of the Hough transform that is not visible normally.

FIGURE 2-9 DETECTED PUPIL AND IRIS CIRCLES
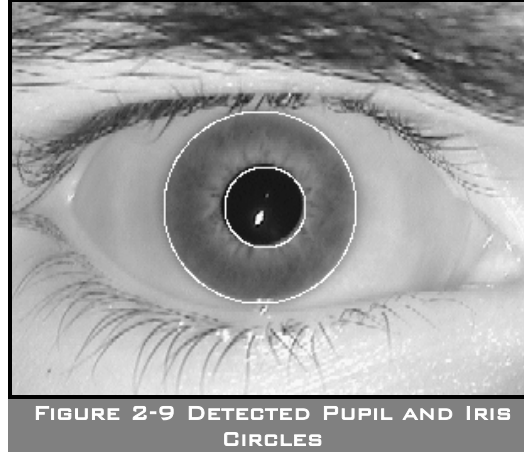
2.2 Optimization

The problem with the technique designed is that it is very slow; it takes about 1.5 minutes to detect both the pupil and iris. This much time is not suitable for a real-time interaction with the user of the system. So some optimizations have been done to improve the performance.

2.2.1 Cross Correlation

In signal processing, cross-correlation is a measure of similarity of two signals, commonly used to find features in an unknown signal by comparing it to a known one. It is a function of the relative time between the signals, is sometimes called the sliding dot product. The correlation of two functions $f(x, y)$ and $h(x, y)$ of the size $M \times N$ is defined as

$$f(x,y) \circ h(x,y) = \frac{1}{MN} \sum_{m=0}^{M-1} \sum_{n=0}^{N-1} f^*(m,n)h(x+m, y+n)$$ Eq: 2-6

where f^* denotes the complex conjugate of f. Here in our case the f i.e. image are real hence $f^* = f$.

Cross correlation technique is used before the Hough transform to have an idea of the where the pupil is in the image. To apply this we simply define a pupil template and cross correlate it with the input image. The cross correlation gives the maximum value and hence a rough estimate of the center of the pupil.

The Hough transform is then performed in the reduced search space for the pupil detection. This reduces the computational time considerably by 4.5 times the time taken otherwise.
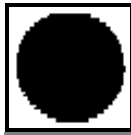
FIGURE 2-10 IRIS TEMPLATE
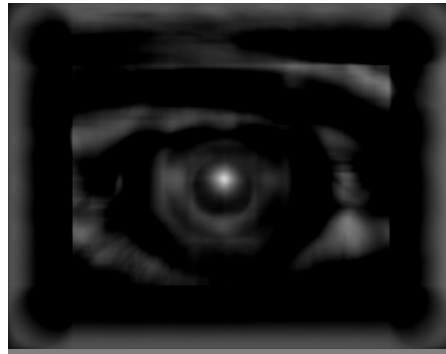
FIGURE 2-11 CORRELATION RESULT
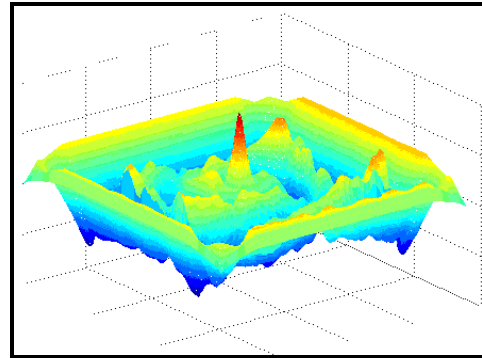
FIGURE 2-12 MESH OF THE CORRELATION

2.2.2 Search Space Reduction Using Prior Knowledge

The conventional Hough transform simply take the whole space to search for the center of the circle. But as we already have the *idea* about the location of the iris/pupil center from the cross correlation hence we don't need to search the whole space for the center, instead just concentrate on the region around which we already have the guess that the center lies. So what we do in this technique is that when we find an edge point, instead of plotting a whole circle around the point we just draw a curve in a limited angle range in the direction for which already have the idea the center lies. This reduces the searching angle from 360° to just 45°, reducing the time by 8 times. The following figure illustrates the difference between the use of Hough transform when used without optimization and the when used with the optimization.
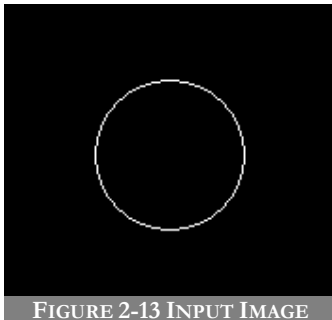
FIGURE 2-13 INPUT IMAGE
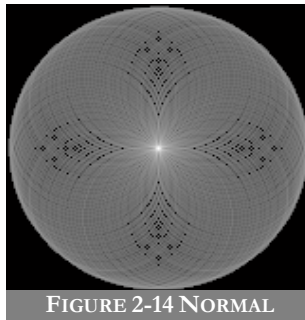
FIGURE 2-14 NORMAL HOUGH TRANSFORM
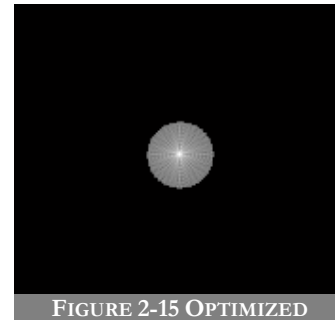
FIGURE 2-15 OPTIMIZED HOUGH TRANSFORM

2.2.3 Search Space Reduction Using Smart Data Extraction

Once the pupil has been detected then we know that the iris is around the pupil hence we extract the data from the edge image in a circular fashion instead of the simple linear manner. This scheme reduces the search to a certain region effectively reducing the computational cost

FIGURE 2-16 OPTIMIZED IRIS SEARCHING
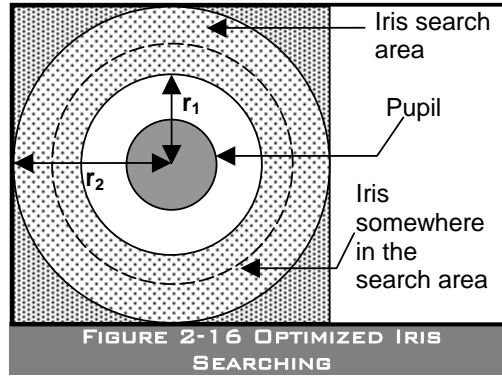
The area to be searched is reduced to just

$$\pi(r_2^2 - r_1^2)$$

Eq: 2-7

where 'r_1' and 'r_2' are the radii of the circles within which the search space if bounded.

2.2.4 Results

Some of the results of the segmentation are given in the Fig. 2.17:

FIGURE 2-17 SEGMENTATION RESULTS
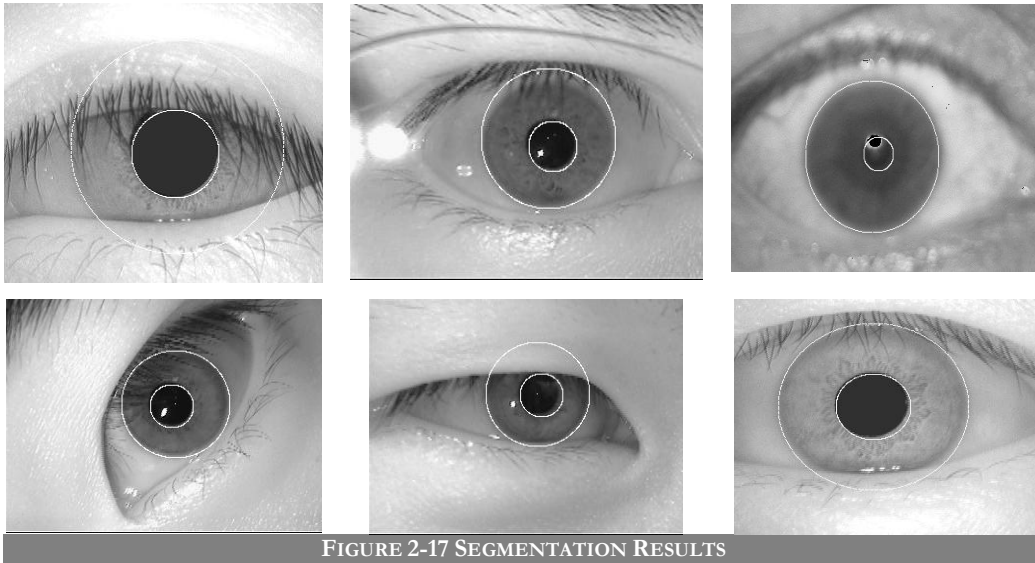
2.3 Normalization

Once the iris region is successfully segmented from an eye image, the next stage is to transform the iris region so that it has fixed dimensions in order to allow comparisons. The dimensional inconsistencies between eye images are mainly due to the stretching of the iris caused by pupil dilation from varying levels of illumination. Other sources of inconsistency include, varying imaging distance, rotation of the camera, head tilt, and rotation of the eye within the eye socket. The normalization process will produce iris regions, which have the same constant dimensions, so that two photographs of the

same iris under different conditions will have characteristic features at the same spatial location.

2.3.1 Daugman's Rubber Sheet Model

The homogenous rubber sheet model devised by Daugman [6] remaps each point within the iris region to a pair of polar coordinates (r, θ) where 'r' is on the interval [0,1] and 'θ' is angle [0, 2π].

FIGURE 2-18 NORMALIZATION FROM THE NON CONCENTRIC CIRCLES

FIGURE 2-19 DAUGMAN'S RUBBER SHEET MODEL
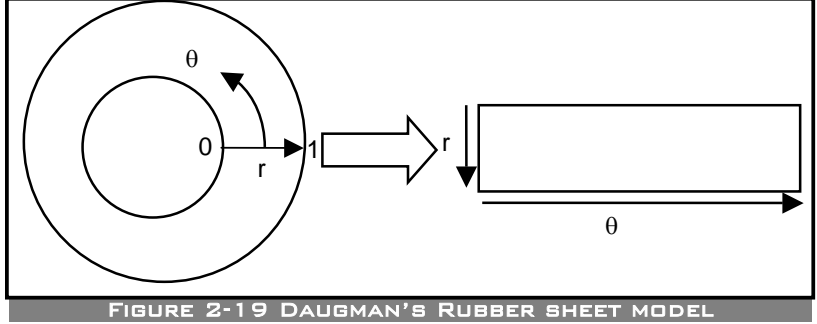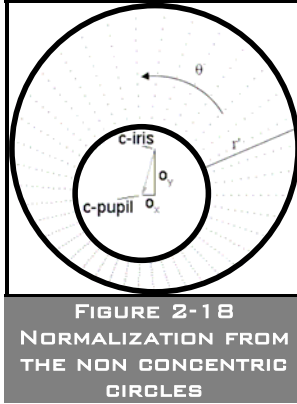
The remapping of the iris region from (x, y) Cartesian coordinates to the normalized non-concentric polar representation is modeled as

$$I(x(r,\theta), y(r,\theta)) \rightarrow I(r,\theta) \qquad \text{Eq: 2-8}$$

with

$$x(r,\theta) = (1-r)x_p(\theta) + rx_i(\theta) \qquad \text{Eq: 2-9}$$
$$y(r,\theta) = (1-r)y_p(\theta) + ry_i(\theta) \qquad \text{Eq: 2-10}$$

where $I(x, y)$ is the iris region image, (x, y) are the original Cartesian coordinates, (r,θ) are the corresponding normalized polar coordinates, and are the coordinates of the pupil and iris boundaries along the 'θ' direction; 'x_i' and 'x_p' are the projections of the circles of iris and pupil in the 'θ' direction, similarly for 'y_i' and 'y_p'. These projections can be given as follows

$$x_p(\theta) = x_{p_o} + r_p \cos(\theta) \qquad \text{Eq: 2-11}$$
$$y_p(\theta) = y_{p_o} + r_p \sin(\theta) \qquad \text{Eq: 2-12}$$
$$x_i(\theta) = x_{io} + r_i \cos(\theta) \qquad \text{Eq: 2-13}$$
$$y_i(\theta) = y_{io} + r_i \sin(\theta) \qquad \text{Eq: 2-14}$$

where 'r_p' and 'r_i' are the radii of pupil and iris, and (x_{po}, y_{po}) and (x_{io}, y_{io}) are the center coordinates of pupil and iris respective.

The rubber sheet model takes into account pupil dilation and size inconsistencies in order to produce a normalized representation with constant dimensions. In this way

the iris region is modeled as a flexible rubber sheet anchored at the iris boundary with the pupil center as the reference point.

FIGURE 2-21 NORMALIZED IMAGE
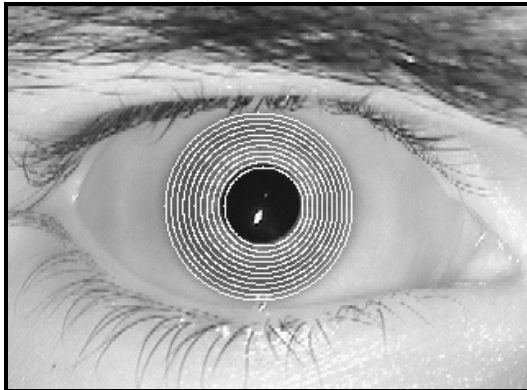
FIGURE 2-20 IRIS EXTRACTION PROCESS

2.3.1.1 Implementation specifications

For different databases there are different radii of the circles and hence the parameters for a number of operations need to be selected. For CASIA and UBIRIS database the radial resolution has been set at 131 and angular resolution at 722. Hence we have a normalized image of 722×131. For MMU database the dimensions are 360×60, as these images are small as compared to the other two databases.

One important point to be mentioned here is that the starting angle of 90° has been selected for normalization, because if we start from the 0° then the occlusion of the lower eyelid breaks into two parts and hence require more computation for the detection of occlusion.

2.4 Eye Occlusion

The major problem in the recognition of the eye is the occlusion of some part of the eye due to the eyelids. To overcome this problem we need to know the portions of the eye that have been occluded. The occlusion detection is generally performed before the normalization step. In the conventional technique an ellipse is fit on the eyelids and the area of the circles i.e. iris and pupil, detected earlier, that has been occluded is found, and hence the area of the eye covered by the eyelids is determined. But this approach has some shortcomings like

- A very large search space to look for.
- Too much of the noise of eyelashes may be present that may at least degrade the performance by increasing the amount of computations to be carried out.

- Eyelids may not form a very well shaped ellipse and sometimes due to lake of intensity difference the edge of the eyelid is not present in the edge detected image.
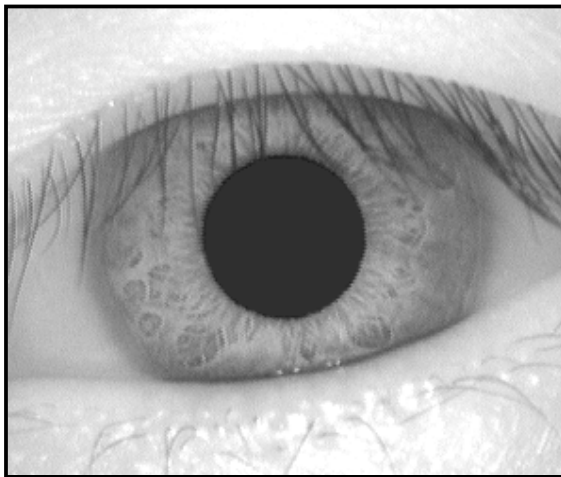
FIGURE 2-22 OCCLUDED IMAGE
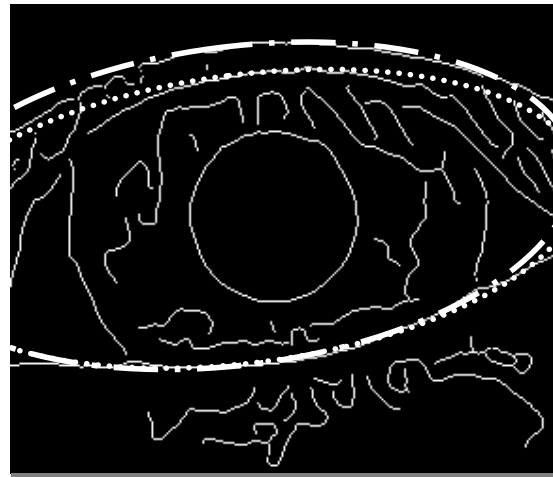
FIGURE 2-23 TWO MOST PROBABLE ELLIPSES FITTED ON THE BOUNDARIES OF THE EYELIDS

In figure 2-20, we have one of the worst case scenarios. From the edge detected image we can see that the upper eyelash area is corrupted due to noise and the edges are not pronounced. Only the lower eyelid portion is properly visible and hence this will influence the parameter selection of the ellipse more than any other.

Two approximations of the ellipses are shown in the edge detected image; none of them is even closer to perfection. The outer ellipse which will be the natural result of maximum voting in Hough space is absolutely a wrong ellipse to fit, as the eye is still occluded due to the lower portion of the upper eyelid. Even if the ellipse is forced to fit the lower portion of the upper eyelid, even then it is not giving a very good approximation as it is leaving a large amount of the area that is occluded.

2.4.1 Optimal Occlusion Detection

A robust solution to this problem has been devised here. In this we detect the occluded area after the normalization process, as it reduces the search space considerably, due to localization of the occlusion with a certain range of the image. The occlusion takes the form of a circle hence it becomes very simple to detect. Noise effect is no more pronounced, as the occlusion portion is below the eyelashes in the normalized image.

As we can see from the normalized image that the occlusion forms a semicircle, which can easily be detected by using circular Hough Transform.
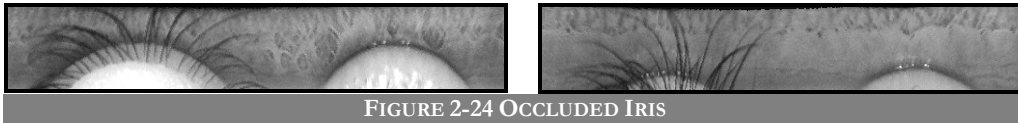
FIGURE 2-24 OCCLUDED IRIS
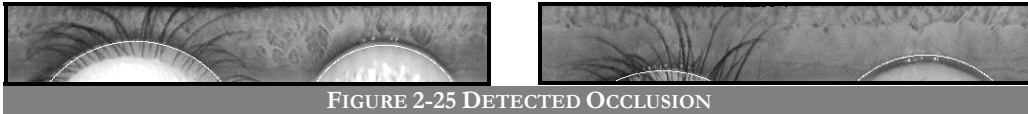
FIGURE 2-25 DETECTED OCCLUSION

2.4.1.1 Implementations Specifications

The nature of the problem simplifies considerably, when we treat it after normalization. We can take the advantage of specific knowledge to optimize the performance of the detection. The following strategies have been adopted to optimize the performance

- As the normalized image is rather large one, hence we scale it down without loosing any useful information that may effect the edge information.

- The upper eyelid and lower eyelid occlusion if present will be within a certain range of the image. As we know that the upper eyelid will always lie to the left half of the normalized image. So we can select a range of the image to fix it for the search of the upper eye occlusion.

- If we observe closely then we can see that wherever the center of this semicircle is it will make an angle of about 45$^\text{o}$ and an angle of -45$^\text{o}$ with the with the left edge and the right edge of the eyelid with respect to the x-axis. So linear transformation has been applied such that it changes the central angle from 45$^\text{o}$ to -45$^\text{o}$ as we move from the left edge to the right edge. Now Hough circle projections are done in the direction of this central angle and hence concentrate around the center of the circle in voting, reducing the computations considerably.

- We can optimize for the '*x*' and '*y*'-component of the center of the circle, as we already know that it is a semicircle and it lies with a certain range of the image, hence its center can not drift too much. So we can put bounds on the '*x*' and '*y*'-axis while voting and also optimize the search to look only in a certain range.

Chapter 3

FEATURE EXTRACTION

The most important stage of the all, this is what for what the whole previous processing steps were done. Some of the features and their types we discuss and illustrated in chapter 1. We can see that these features are so divergent, enormous and difficult to locate if treated separately and such a scheme will be extremely inefficient. Therefore unlike the feature extraction methods of fingerprint in which we locate the bifurcations and ridge endings, here we treat the iris as a texture. This gives us a way to look at the problem from another perspective; it requires a very good knowledge of texture analysis to solve the problem.

There are lots of tools and techniques employed for texture analysis, but here out aim is feature extraction. Hence feature extraction will be the main focus of the discussion. Different techniques that have been employed for the iris feature extraction include phase based methods [4][5][6], wavelet zero-crossing method[30], and texture analysis methods[27][28].

We start with the formal definition of texture and then move on to different techniques for feature extraction.

3.1 Texture

Textures are patterns though very easily judged visually but extremely difficult to quantify it technically. There exists no very well accepted definition of texture. Some authors have attempted to qualitatively define the texture. Pickett [14] states that

> "texture is used to describe two dimensional arrays of variations…
> The elements and rules of spacing or arrangement may be arbitrarily
> manipulated, provided a characteristic repetitiveness remains."

Hawkins [14] has given a more detailed description of texture:

> "The notion of texture appears to depend upon three ingredients: 1.
> some local 'order' is repeated over a region which is large in
> comparison to the order's size, 2. the order consists in the nonrandom
> arrangement of elementary parts and 3. the parts are roughly uniform
> entities having approximately the same dimensions everywhere
> within the textured region."

Lohse indicates that people are sensitive to three texture properties: repetition, directionality and complexity [28].

3.2 Filter Bank Techniques

Based on Human Visual System (HVS) investigation a model for the HVS interpretation of texture has been based on multi-channel filtering of narrow bands. Simple cells in the visual cortex are found to be sensitive to different channels of combinations of various spatial frequencies and orientations. Since texture repetition can be characterized by its spatial frequency, and directionality by its orientation, then we can fit the HVS model into a methodology that uses multi-channel filtering at different spatial-frequencies and orientation for texture analysis.

3.2.1 Gabor Filters

Gabor filters are mostly used as the channel filters. The Gabor filters are band-pass filters with tunable center frequency, orientation and bandwidth.

Gabor filters have the ability to perform multi-resolution decomposition due to to its localization both in spatial and spatial-frequency domain. Filters with smaller bandwidths in the spatial-frequency domain are more desirable because they allow us to make finer distinction among different textures. On the other hand, accurate localization of texture boundaries requires filters that are localized in spatial domain.

However, normally the effective width of a filter in the spatial domain and its bandwidth in the spatial-frequency domain are inversely related according the uncertainty principle that is why Gabor filters are well suited for this kind of problem. A Gabor function in the spatial domain is a sinusoidal modulated Gaussian. For a 2-D Gaussian curve with a spread of 'σ_x' and 'σ_y' and a modulating frequency of u_o and v_o in the 'x' and 'y' directions, respectively. The two dimensional form of Gabor filter is given by

$$G(x, y; \theta, f) = \frac{1}{2\pi\sigma_x\sigma_y} \exp\left\{-\frac{1}{2}\left[\frac{x'^2}{\sigma_x^2} + \frac{y'^2}{\sigma_y^2}\right]\right\} \exp(j2\pi(ux + vy)) \qquad \text{Eq: 3-1}$$

with spatial frequency $f = \sqrt{u_o^2 + v_o^2}$ and direction $\theta = \tan^{-1}\left(\dfrac{v_o}{u_o}\right)$. This function can be split into two parts, then even and odd filters $h_e(x, y)$ and $h_o(x, y)$ which are also called symmetric and antisymmetric filter respectively. This filter pair is given as

$$G_e(x, y; \theta, f) = \frac{1}{2\pi\sigma_x\sigma_y} \exp\left\{-\frac{1}{2}\left[\frac{x'^2}{\sigma_x^2} + \frac{y'^2}{\sigma_y^2}\right]\right\} \cos(2\pi f x') \qquad \text{Eq: 3-2}$$

$$G_o(x, y; \theta, f) = \frac{1}{2\pi\sigma_x\sigma_y} \exp\left\{-\frac{1}{2}\left[\frac{x'^2}{\sigma_x^2} + \frac{y'^2}{\sigma_y^2}\right]\right\} \sin(2\pi f x') \qquad \text{Eq: 3-3}$$

where

$$x' = x\cos\theta + y\sin\theta \qquad \text{Eq: 3-4}$$
$$y' = -x\sin\theta + y\cos\theta \qquad \text{Eq: 3-5}$$
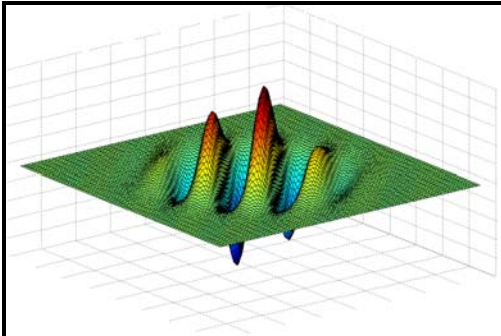
FIGURE 3-1 ODD SYMMETRIC GABOR FILTER
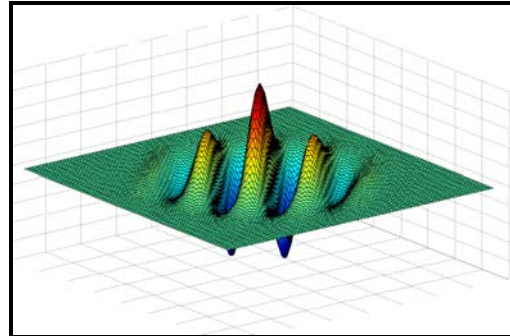
FIGURE 3-2 EVEN SYMMETRIC GABOR FILTER

FIGURE 3-3 FREQUENCY RESPONSE OF GABOR FILTER

FIGURE 3-4 ANOTHER VIEW OF FREQUENCY RESPONSE
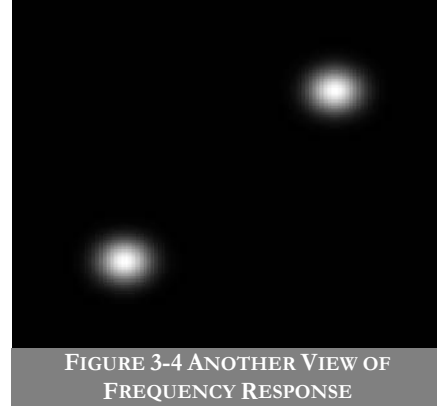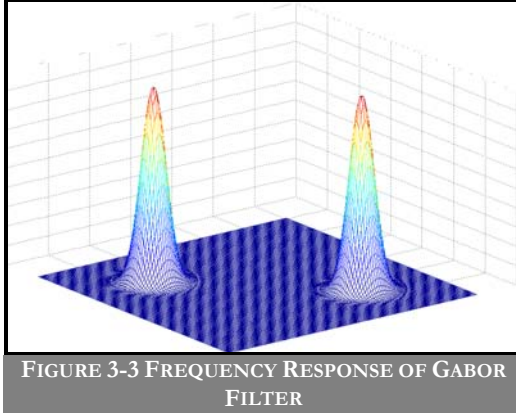
The frequency 'f' and angle 'θ' define the center location of the filter. By tuning the 'f' and 'θ' to different center locations we can create multiple filters that cover the spatial-frequency domain. However, another important aspect of the filter is the frequency bandwidth B_F and the orientation B_θ. These can be set to constant values that match psycho visual data [28]. In particular a frequency bandwidth of 1 octave is found to perform well. The frequency bandwidth, in octaves, from frequency f_1 to frequency f_2, is given by $\log_2(f_2/f_1)$. It has to be noted that the frequency bandwidth increases with frequency in a logarithmic fashion. An orientation bandwidth of 30° is recommended by Clausi and Jernigan[28].

3.2.1.1 Feature Extraction

In texture segmentation different feature like the magnitudes of the filter response or moments are calculated, but here our aim is not segmentation, we want to determine some quantities such that when same different irides are compared then these features (quantities) should be able to differentiate the two.

So many different schemes can be figured out like mean and standard deviation based scheme. In this scheme the filter is tuned at certain frequencies like the values that has been used at the in my work f = 2, 4, 8, 16, 32 and 64 cycles/degree and orientations θ = 0°, 45°, 90° and 135°. This leads to a total 24 images, from which the iris features are extracted. These features are the mean and the standard deviation of each output image. Therefore, 48 features per input image are calculated. This scheme inherently becomes rotation invariant.

We can further take this scheme one step ahead. We can divide the normalized image into subimages vertically. Now the filter bank is designed exactly in the same way

and convolved with the image. If we take the same parameters as defined in the previous case we will get total of 192 features (24 images * 8 subimage). The sub images can be coded as features as average absolute deviation, given as

$$V = \frac{1}{N}\left(\sum_N |f(x,y) - m|\right) \qquad \text{Eq: 3-6}$$

where 'N' is the number of pixels in the image, m is the mean of the image, and $f(x,y)$ is the value at point (x, y).

3.2.2 Circular Symmetric Filters

In this method circular symmetric Gabor filters are used instead of general Gabor filters. The difference between the two lies in the modulating sinusoidal function. The Gabor filter is modulated by an oriented sinusoidal function, whereas circular symmetric filter (CSF) is modulated by a circular symmetric sinusoidal function. A CSF is defined as follows:

$$G(x,y,f) = \frac{1}{2\pi\sigma_x\sigma_y}\exp\left\{-\frac{1}{2}\left[\frac{x^2}{\sigma_{x'}^2} + \frac{y^2}{\sigma_{y'}^2}\right]\right\}\exp(j2\pi f\sqrt{x^2 + y^2}) \qquad \text{Eq: 3-7}$$

where 'f' is the central frequency of a circular Gabor filter.

The responses of the filter are as follows
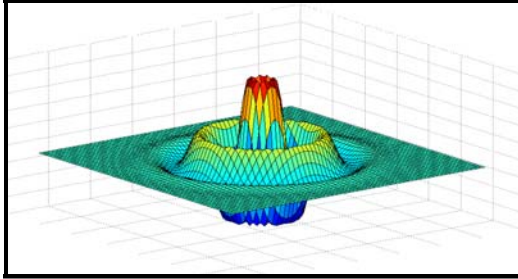
FIGURE 3-5 ODD SYMMETRIC CIRCULAR GABOR FILTER
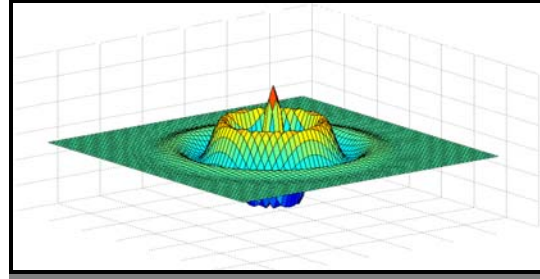
FIGURE 3-6 EVEN SYMMETRIC CIRCULAR GABOR FILTER
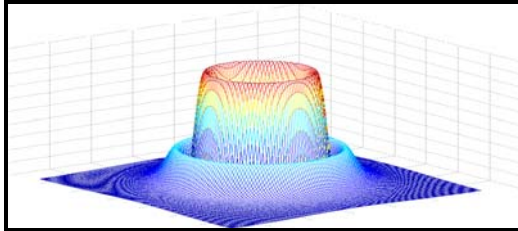
FIGURE 3-7 FREQUENCY RESPONSE OF ODD SYMMETRIC FILTER
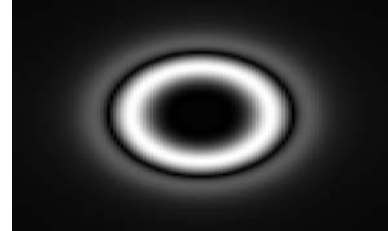
FIGURE 3-8 FREQUENCY RESPONSE OF ODD SYMMETRIC FILTER

3.2.2.1 Feature Extraction

Feature extraction through CSF is essentially the same as the Gabor filter technique. We can adopt any of the techniques that are mentioned in the Gabor filter technique.

3.3 Wavelet Transform

3.3.1 Introduction

Wavelet transform is the technique that has been finally Before we discuss anything about the wavelet transform, a few words about the motivation towards the wavelet transform are worth mentioning.

3.3.2 Fourier Transform

Fourier transform can be defined as

"An integral transform that re-expresses a function in terms of sinusoidal basis functions, i.e. as a sum or integral of sinusoidal functions multiplied by some coefficients ("amplitudes").

This transform can be achieved as follows

$$X(f) = \int_{-\infty}^{\infty} x(t)e^{-j2\pi ft}dt \qquad\qquad \text{Eq: 3-8}$$

$$x(t) = \int_{-\infty}^{\infty} X(f)e^{j2\pi ft}df \qquad\qquad \text{Eq: 3-9}$$

These two equations are called the Fourier transform pair. We can see that the signal $x(t)$, is multiplied with an exponential term, at a certain frequency "f" , and then integrated over all times. If the result of this integration is a large value, then we say that the signal $x(t)$, has a dominant spectral component at frequency "f". This means that, a major portion of this signal is composed of frequency 'f'. If the integration result is a small value, than this means that the signal does not have a major frequency component of 'f' in it. If this integration result is zero, then the signal does not contain the frequency 'f' at all.

The all times notion signifies that no matter where in time the component with frequency 'f' appears, it will affect the result of the integration equally as well. This is why Fourier transform is not suitable if the signal has time varying frequency. If only, the signal has the frequency component 'f' at all times, then the result obtained by the Fourier transform makes sense. Note that the Fourier transform tells whether a certain frequency component exists or not. This information is independent of where in time this component appears.

3.3.3 Short Term Fourier transform

To overcome this limitation of Fourier transform Short Term Fourier Transform (STFT) was introduced. In this the signal is broken into slots of fixed length of time with the help of a window and then the Fourier transform is taken. Though it solves the time-frequency problem to some extent, but it has limitation that it takes a window of fixed size, which may be inapplicable to a varying frequency (non-stationary) signal. STFT is given by

$$STFT_X^{(\omega)}(t,f) = \int_t \left[x(t) \omega^*(t-t') \right] e^{-j2\pi ft} dt$$

Eq: 3-10

In FT there is no resolution problem in the frequency domain, i.e., we know exactly what frequencies exist; similarly we there is no time resolution problem in the time domain, since we know the value of the signal at every instant of time. Conversely, the time resolution in the FT, and the frequency resolution in the time domain are zero, since we have no information about them. What gives the perfect frequency resolution in the FT is the fact that the window used in the FT is its kernel, the e^{jwt} function, which lasts at all times from minus infinity to plus infinity. Now, in STFT, our window is of finite length, thus it covers only a portion of the signal, which causes the frequency resolution to get poorer. What I mean by getting poorer is that, we no longer know the exact frequency components that exist in the signal, but we only know a band of frequencies that exist. This time frequency resolution problem with STFT is the fact whose roots go back to what is known as the Heisenberg Uncertainty Principle**.**

3.3.4 Continuous Wavelet Transform (CWT)

The continuous wavelet transform was developed as an alternative approach to the short time Fourier transform to overcome the resolution problem. The wavelet analysis is done in a similar way to the STFT analysis, in the sense that the signal is multiplied with a function, similar to the window function in the STFT, and the transform is computed separately for different segments of the time-domain signal. However, there are two main differences between the STFT and the CWT

1. The Fourier transforms of the windowed signals are not taken, and therefore single peak will be seen corresponding to a sinusoid, i.e., negative frequencies are not computed.

2. The width of the window is changed as the transform is computed for every single spectral component, which is probably the most significant characteristic of the wavelet transform.

Fourier analysis consists of breaking up a signal into sine waves of various frequencies. Similarly, wavelet analysis is the breaking up of a signal into shifted and scaled versions of the original (or *mother*) wavelet.

Often times a particular spectral component occurring at any instant can be of particular interest. In these cases it may be very beneficial to know the time intervals these particular spectral components occur. *It also makes sense that local features can be described better with wavelets that have local extent.*

The continuous wavelet transform is defined as follows

$$CWT_x^\psi(\tau,s) = \Psi_x^\psi(\tau,s) = \frac{1}{\sqrt{|s|}}\int x(t)\psi *\left(\frac{t-\tau}{s}\right)dt \qquad \text{Eq: 3-11}$$

As seen in the above equation, the transformed signal is a function of two variables, 'τ' and 's' , the translation and scale parameters, respectively. $\psi(t)$ is the transforming function, and it is called the mother wavelet . The mother wavelet is a **prototype** for generating the other window functions.

3.3.4.1 Translation

The term **translation** is related to the location of the window, as the window is shifted through the signal. This term, obviously, corresponds to time information in the transform domain. However, we do not have a frequency parameter, as we had before for the STFT.
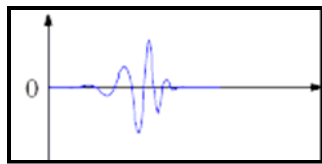
FIGURE 3-9 WAVELET AT ZERO TRANSLATION
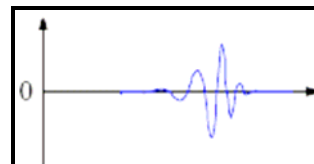
FIGURE 3-10 TRANSLATED WAVELET

3.3.4.2 The Scale

The parameter **scale** in the wavelet analysis is similar to the scale used in maps. As in the case of maps, high scales correspond to a non-detailed global view (of the signal), and low scales correspond to a detailed view. Similarly, in terms of frequency, low frequencies (high scales) correspond to a global information of a signal (that usually spans the entire signal), whereas high frequencies (low scales) correspond to a

detailed information of a hidden pattern in the signal (that usually lasts a relatively short time). Cosine signals corresponding to various scales are given as examples in the following figure.

FIGURE 3-11 SCALING
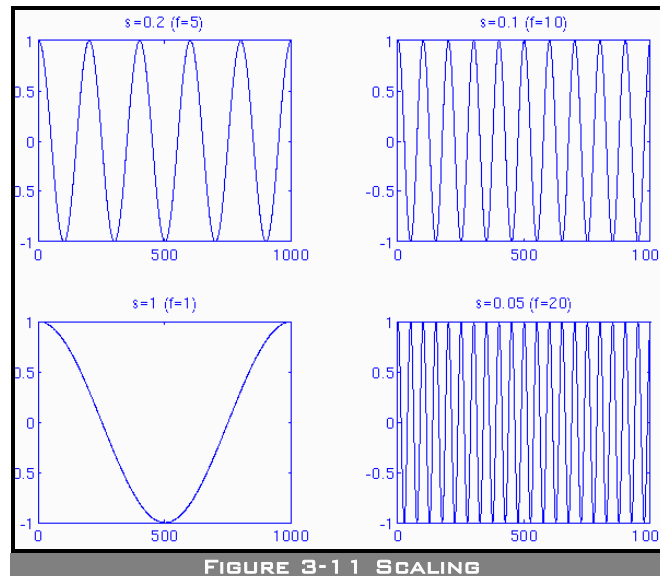
Scaling, as a mathematical operation, either dilates or compresses a signal. Larger scales correspond to dilated (or stretched out) signals and small scales correspond to compressed signals.

3.3.4.3 Computing CWT

To computer a CWT we need to carryout the following steps

1. Take a wavelet and compare it to a section at the start of the original signal.
2. Calculate a number, C, that represents how closely correlated the wavelet is with this section of the signal. The higher C is, the more the similarity. More precisely, if the signal energy and the wavelet energy are equal to one, C maybe interpreted as a correlation coefficient.

C = 0.0102
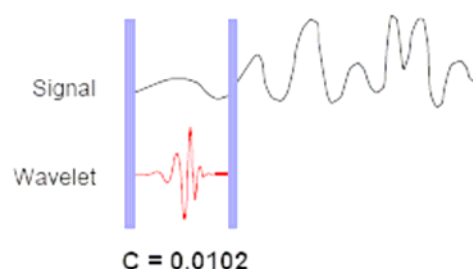
Note that the results will depend on the shape of the wavelet you choose.

3. Shift the wavelet to the right and repeat steps 1 and 2 until you've covered the whole signal.
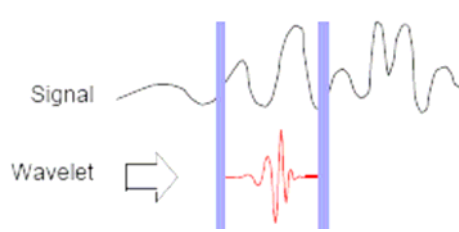
4. Scale (stretch) the wavelet and repeat steps 1 through 3.

C = 0.2247
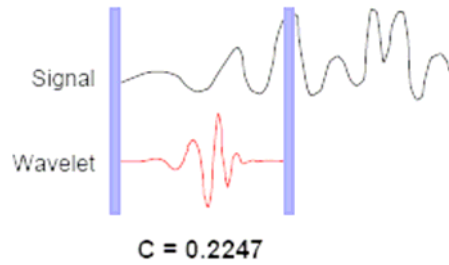
5. Repeat steps 1 through 4 for all scales.

3.3.5 Discrete Wavelet Transform (DWT)

Because of the enormous amount of computation needed to perform the CWT it is important to develop a discrete version. The main idea is the same as it is in the CWT. A time-scale representation of a digital signal is obtained using digital filtering techniques. In the discrete case, filters of different cutoff frequencies are used to analyze the signal at different scales. The signal is passed through a series of high pass filters to analyze the high frequencies, and it is passed through a series of low pass filters to analyze the low frequencies.

The resolution of the signal, which is a measure of the amount of detail information in the signal, is changed by the filtering operations, and the scale is changed by upsampling and downsampling (subsampling) operations. Subsampling a signal corresponds to reducing the sampling rate, or removing some of the samples of the signal.

Although it is not the only possible choice, DWT coefficients are usually sampled from the CWT on a dyadic grid i.e. power of two. Since the signal is a discrete time function, the terms function and sequence will be used interchangeably in the following discussion. This sequence will be denoted by $x[n]$, where 'n' is an integer.

The procedure starts with passing this signal (sequence) through a half band digital lowpass filter with impulse response $h[n]$. Filtering a signal corresponds to the mathematical operation of convolution of the signal with the impulse response of the filter. The convolution operation in discrete time is defined as follows

$$x[n] * h[n] = \sum_{k=-\infty}^{\infty} x[k].h[n-k]$$ Eq: 3-12

A half band lowpass filter removes all frequencies that are above half of the highest frequency in the signal.

The unit of frequency is of particular importance at this time. In discrete signals, frequency is expressed in terms of radians. Accordingly, the sampling frequency of the signal is equal to 2π radians in terms of radial frequency. Therefore, the highest frequency component that exists in a signal will be π radians, if the signal is sampled at Nyquist's rate; that is, the Nyquist's rate corresponds to π rad/s in the discrete frequency domain.

After passing the signal through a half band lowpass filter, half of the samples can be eliminated according to the Nyquist's rule, since the signal now has a highest frequency of $\pi/2$ radians instead of π radians. Simply discarding every other sample will **subsample** the signal by two, and the signal will then have half the number of points. The scale of the signal is now doubled. Note that the lowpass filtering removes the high frequency information, but leaves the scale unchanged. Only the subsampling process changes the scale. Resolution, on the other hand, is related to the amount of information in the signal, and therefore, it is affected by the filtering operations. Half band lowpass filtering removes half of the frequencies, which can be interpreted as losing half of the information. Therefore, the resolution is halved after the filtering operation. Note, however, the subsampling operation after filtering does not affect the resolution, since removing half of the spectral components from the signal makes half the number of samples redundant anyway. Half the samples can be discarded without any loss of information. In summary, the lowpass filtering halves the resolution, but leaves the scale unchanged. The signal is then subsampled by 2 since half of the number of samples are redundant. This doubles the scale.

This procedure can mathematically be expressed as

$$y[n] = \sum_{k=-\infty}^{\infty} h[k].x[2n-k]$$ Eq: 3-13

The DWT analyzes the signal at different frequency bands with different resolutions by decomposing the signal into a coarse approximation and detail information. DWT employs two sets of functions, called scaling functions and wavelet functions, which are associated with low pass and highpass filters, respectively. The decomposition of the signal into different frequency bands is simply obtained by successive highpass

and lowpass filtering of the time domain signal. The original signal x[n] is first passed through a halfband highpass filter $g[n]$ and a lowpass filter $h[n]$. After the filtering, half of the samples can be eliminated according to the Nyquist's rule, since the signal now has a highest frequency of $\pi/2$ radians instead of π. The signal can therefore be subsampled by 2, simply by discarding every other sample. This constitutes one level of decomposition and can mathematically be expressed as follows:

$$y_{high}[k] = \sum_n x[n].g[2k-n]$$ Eq: 3-14

$$y_{low}[k] = \sum_n x[n].h[2k-n]$$ Eq: 3-15

where $y_{high}[k]$ and $y_{low}[k]$ are the outputs of the highpass and lowpass filters, respectively, after subsampling by 2.

This decomposition halves the time resolution since only half the number of samples now characterizes the entire signal. However, this operation doubles the frequency resolution, since the frequency band of the signal now spans only half the previous frequency band, effectively reducing the uncertainty in the frequency by half. The above procedure, which is also known as the *subband coding*, can be repeated for further decomposition. At every level, the filtering and subsampling will result in half the number of samples (and hence half the time resolution) and half the frequency band spanned (and hence double the frequency resolution). Figure 3.14 illustrates this procedure, where *x[n]* is the original signal to be decomposed, and *h[n]* and *g[n]* are lowpass and highpass filters, respectively. The bandwidth of the signal at every level is marked on the figure as '*f*'.

FIGURE 3-12 SUBBAND CODING
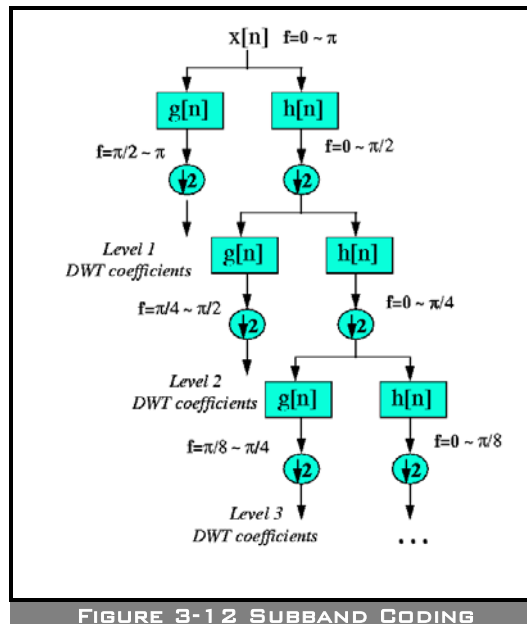
3.3.5.1 Iris Feature Extraction

The iris feature extraction process can be illustrated in figure 3.15

Figure 3-13 Wavelet Transformation scheme of the iris image
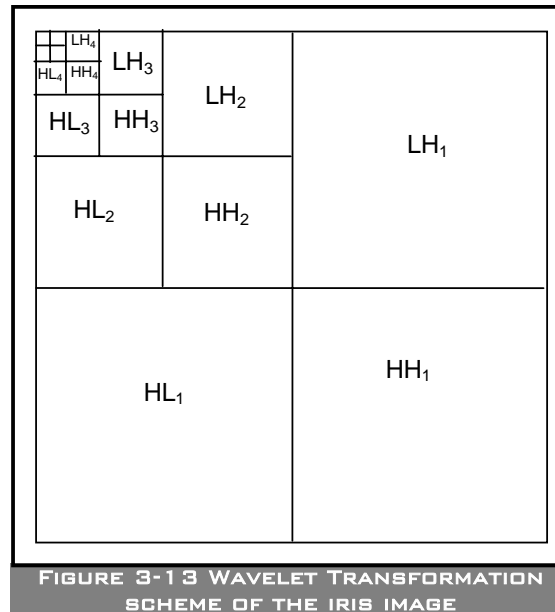
Here '*H*' and '*L*' mean the high pass and low pass filters respectively. While rest of the scheme is same for taking the wavelet transform, the only difference is that this is performed in two dimensions instead of just one.

For the wavelet transform 'Haar' wavelet has been selected. We obtain the 5-level wavelet tree showing all detail and approximation coefficients of one mapped image obtained from the mapping part. When comparing the results using the Haar transform with the wavelet tree obtained using other wavelets the results of the Haar wavelet were slightly better.

Figure 3-14 Harr Wavelet
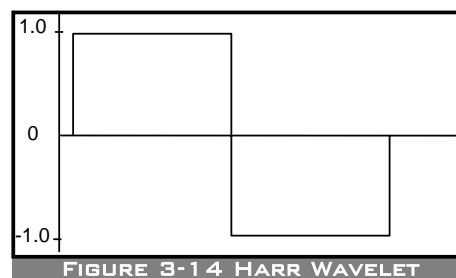
Our mapped image can be decomposed using the Haar wavelet into a maximum of five levels. We must now pick up the coefficients that represent the core of the iris pattern. Therefore those that reveal redundant information should be eliminated.

When analyzed the patterns HH_1, HH_2, HH_3 and HH_4 h are almost the same and only one can be chosen to reduce redundancy.

Since HH_4 repeats the same patterns as the previous horizontal detail levels and it is the smallest in size, then we can take it as a representative of all the information the four levels carry. In a similar fashion, only the fourth vertical and diagonal coefficients can be taken to express the characteristic patterns in the iris-mapped image. Thus we can represent each image applied to the Haar wavelet as the combination of three matrices:

- HH_4 HH_5
- HL_4 HL_5
- LH_4 LH_5

All these matrices are combined to build one single vector characterizing the iris patterns. This vector is called the feature vector [4]. For MMU database the normalized images have a fixed size of 360×60 then all images will have a fixed feature vector. In our case, this vector has a size of 348 elements. For CASIA and UBIRIS the input image is 722×131, and the resulting feature vector length is 1587 elements.

It is very important to represent the obtained vector in a binary code because it is easier to find the difference between two binary code-words than between two number vectors. In fact, Boolean vectors are always easier to compare and to manipulate. In order to code the feature vector should first be observed for some of its characteristics. It is found that all the vectors that is obtained have a maximum value that is greater than 0 and a minimum value that is less than 0.

If "Coef" is the feature vector of an image than the following quantization scheme converts it to its equivalent code-word:

$$\text{If Coef(i) >= 0 then Coef(i) = 1}$$
$$\text{If Coef(i) < 0 then Coef(i) = 0}$$

The next step is to compare two code-words to find out if they represent the same person or not.

3.4 Feature Matching

3.4.1 Hamming Distance

The Hamming distance gives a measure of how many bits are the same between two bit patterns. Using the Hamming distance of two bit patterns, a decision can be made as to whether the two patterns were generated from different irises or from the same one.

In comparing the bit patterns X and Y, the Hamming distance, HD, is defined as the sum of disagreeing bits (sum of the exclusive-OR between X and Y) over N, the total number of bits in the bit pattern

$$HD = \frac{1}{N}\sum_{j=1}^{N} X_j (XOR) Y_j$$ Eq: 3-16

Since an individual iris region contains features with high degrees of freedom, each iris region will produce a bit-pattern which is independent to that produced by another iris, on the other hand, two iris codes produced from the same iris will be highly correlated.

John Daugman, the pioneer in iris recognition conducted his tests on a very large number of iris patterns (up to 3 million iris images) and deduced that the maximum Hamming distance that exists between two irises belonging to the same person is 0.32 [4].
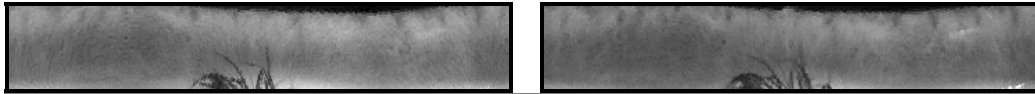
FIGURE 3-15 TWO NORMALIZED IMAGES OF THE SAME EYE.

The hamming distance for the above two normalized images of the save eye is .119565, hence identifying the person correctly.

3.4.2 Camera Defocusing Immunity

Defocusing of the camera does not effect the results at all, upto a great extent.

If we apply Gaussian blur to the following image and find the hamming distance after extracting feature. The distance is just 0.010870, we can see that it almost does not effect the recognition process.
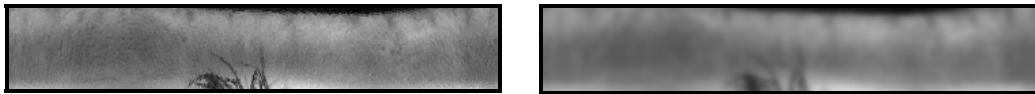
FIGURE 3-16 THE NORMALIZED AND THE BLURRED VERSION OF THE IMAGE.

3.4.3 Noise Immunity

The system's performance is robust to the noise until it does not corrupt the information more than 30%. The HD between the two normalized images of the same eye is just 14.49%.
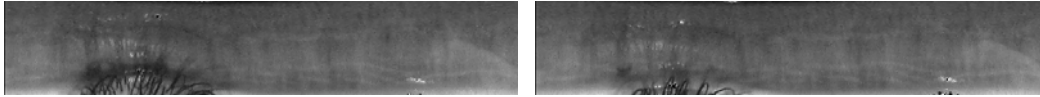
FIGURE 3-17 NOISE IMMUNITY

3.4.4 Head Rotation Invariance

The head rotation is easily compensated by rotating the code template by right and left shifting for a limited number of bits. This shifting is equivalent to the rotation of the input image. The HD between the following two images if 22.22%.
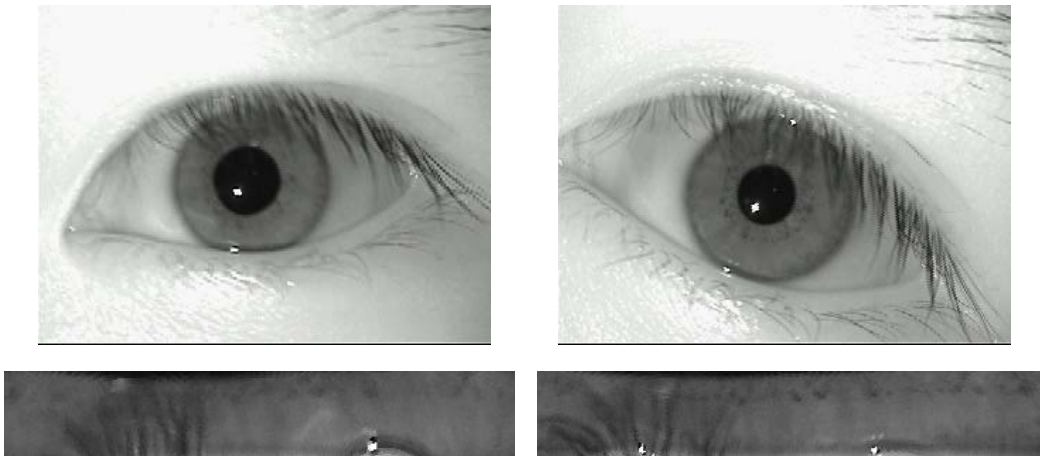
FIGURE 3-18 HEAD ROTATIN INVARIANCE

3.4.5 Eye occlusion

Eye occlusion was successfully detected as described in the sections 2.5, now this segmentation will be used in this step. While performing the matching process only the segments of the code that don't belong to the occluded eye should be matched. Hence at the stage of the registration of a person, *occlusion mask* is also stored that describes the areas of the eye which are occluded. One thing should be noted here that this is not a restoration process, as the area that is occluded is lost and we have a reduced amount of information for comparison now, reducing the degrees of freedom. So this should only be done when the occlusion of the eye does not cause too much of the eye information to be lost.

Chapter 4

RESULTS AND DISCUSSIONS

After we have discussed all the algorithms and implementations details, it is important to discuss the accuracy of these algorithms, the ability of these algorithms to discriminate the two persons, and some other issues like robustness the system to imposters and discussing the feature selection procedure in detail.

4.1 Databases

Before carrying out any sort of analysis, its important to discuss about the databases used to carryout this analysis. Basically three databases have been used in this analysis:

1. UBIRIS database

    UBIRIS database is composed of 1877 images collected from 241 persons. It incorporates images with several noise factors, thus permitting the evaluation of robustness iris recognition methodologies.

2. Multimedia University database 1

    MMU1 iris database contributes a total number of 450 iris images of 45 individuals. It contains five images both of the left and the right eye.

Though CASIA database was initially included for testing purpose but as it is rather easy database to work with, hence it was dropped and the two databases mentioned above were used to test the developed system. Statistical analysis is carried out only on the MMU database. The main reason to select this database is that it contains the images of good number of individuals with both the right and left eye, on contrary to the UBIRIS database which contains only right eye image. Apart from that it covers most of the worst cases like head tilting, occlusion, eyelashes and intensity variation etc.

4.2 Code Information Capacity

It is important that there should be independent variation in iris detail, both within a given iris and across the human population. Both the similarity of iris details across the population and within the iris itself would reduce its statistical complexity, or dimensionality, and thus undermine its uniqueness[5].

A code of any length has maximum information capacity if all its possible states are equiprobable [6]. This reflects the fact that the Shannon entropy measure

$$S = -\sum_{j=1}^{n} P_j \log_2 P_j$$

Eq: 4-1

for the probability of each of the *n* states and with

$$\sum_{j=1}^{n} P_j = 1$$

Eq: 4-2

is maximum when for all *j*,

$$P_j = \frac{1}{n}$$

Eq: 4-3

FIGURE 4-1 EQUIPROBABLE IRIS CODE BITS VARIATION
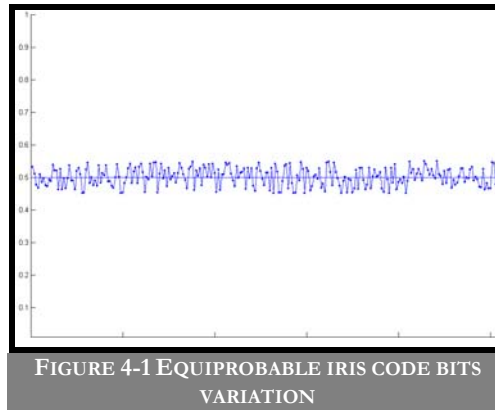
We can see that the graph is fairly equiprobable across all code bit locations, and we can also observe that for each bit *p*=1–*p*, hence giving maximum randomness in the

code. The flatness of the graph reflects the existence of independent variation in the detailed iris texture, both across an iris and across the human population studied. Across the population, the constant independent probability of any given code bit being set presumably reflects the absence of genetic penetrance in the detailed morphogenesis of this tissue, in favor of stochastic or chaotic processes.

4.3 Degrees-of-Freedom in an Iris Code

The code generated in the previous chapter gives lesser degrees of freedom than its actual length, one reason is that there are substantial radial correlations within an iris. For example, a given furrow or ciliary process tends to propagate across a significant radial distance in the iris, exerting its influence on several remote parts of the code, thus reducing their independence. Similarly, a feature such as a furrow influences different parts of the code associated with several different scales of analysis, since the Fourier spectrum of such a punctate feature can span several octaves.

The number of independent degrees-of-freedom in an iris code can be estimated by examining the distribution of Hamming distances computed across a population of unrelated iris codes. Comparing each pair of iris codes *A* and *B* bit-by-bit, their normalized Hamming distance HD is defined in eq: 3-16.

Since each bit of any iris code has equal *a priori* odds of being a 1 or a 0, there is probability *p*=0.5 that any pair of bits from different iris codes disagree. If each of the bits in a given iris code were fully independent of every other bit, then the expected distribution of observed Hamming distances between two independent such iris codes would be a binomial distribution with *p*=0.5.

Therefore uniqueness was determined by comparing templates generated from different eyes to each other, and examining the distribution of Hamming distance values produced. This distribution is known as the inter-class distribution.

The templates are shifted left and right to account for rotational inconsistencies in the eye image, and the lowest Hamming distance is taken as the actual Hamming distance. Due to this, the mean Hamming distance for inter-class template comparisons will be slightly lower than 0.5, since the lowest Hamming distance out of several comparisons between shifted templates is taken. As the number of shifts increases, the mean Hamming distance for inter-class comparisons will decrease accordingly.

Uniqueness was also be determined by measuring the number of degrees of freedom represented by the templates. This gives a measure of the complexity of iris patterns, and can be calculated by approximating the collection of inter-class Hamming distance values as a binomial distribution. The number of degrees of freedom, DOF, can be calculated by

$$DOF = \frac{p(1-p)}{\sigma^2}$$
Eq: 4-4

where 'p' is the mean, and σ is the standard deviation of the distribution.

4.4 Results and Parameter Selection

4.4.1 Preprcessing

The only preprocessing needed normally is the edge detection. For implementation canny edge detector is used with the Gaussian radius of '2' and threshold of '0.1'.

For UBIRIS database gamma correction has been applied at a factor of 0.5 so as to compensate the contrast inconsistency.

4.4.2 Segmentation

The segmentation algorithm takes about 4 sec per image. The developed algorithm successfully segmented 93% of the MMU database images, for UBIRIS it was 88% for session one images, comprising of 1250 images.

4.4.3 Recognition

The performance of the system is evaluated on MMU database. The specifications of this are given as

- 404 out of 450 images of MMU database are used. 10 percent of the images are dropped because either segmentation failed on these images or the eyes are over occluded.

- The images that are subjected to the test also contained some worst case situations, including 27% of the images with more than 40% of the iris area either occluded or covered by the eye lashes, image with too much pupil dilation or too much head tilting. These worst cases are included so as to study the effect of these conditions on the over all performance of the system.

- 10 bit right and left shift is incorporated to compensate the head tilting.

- The evaluation comprises of 739 intra-class i.e. for the same eye, comparisons and 80780 inter-class i.e. different eyes, comparisons.

Some of the worst cases that are included in the test phase are shown in fig. 4.2.
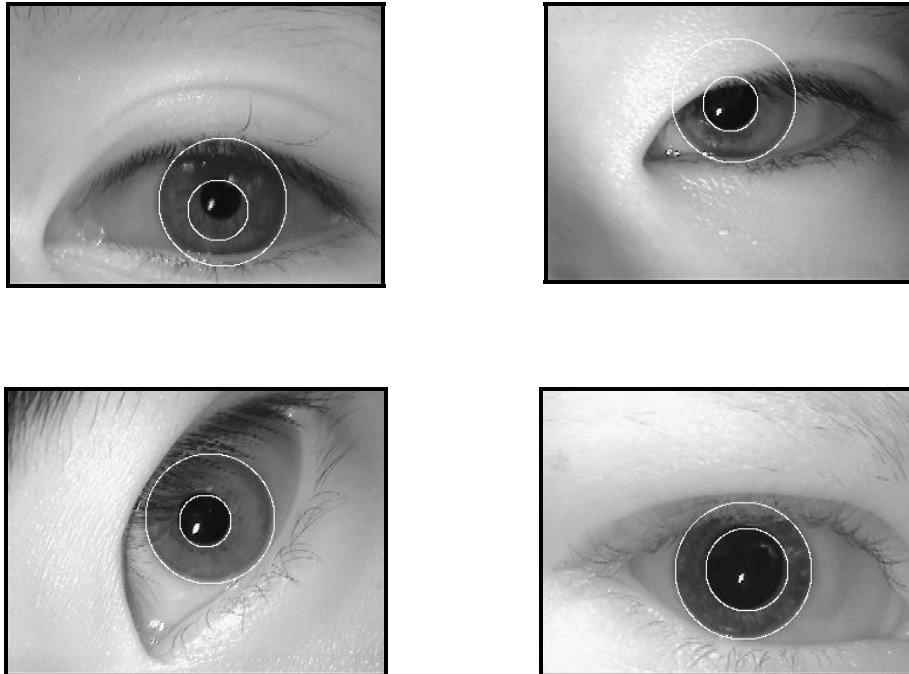
FIGURE 4-2 SOME WORST CASES INCLUDED FOR TEST, INCLUDING OVER OCCLUSION, WRONG SEGMENTATION, EXTREME HEAD TILTING, EXTRA PUPIL DILATION

The result of the inter-class comparisons is shown in fig. 4-3.

Mean = 0.385
St. Dev = 0.033
DOF = 218
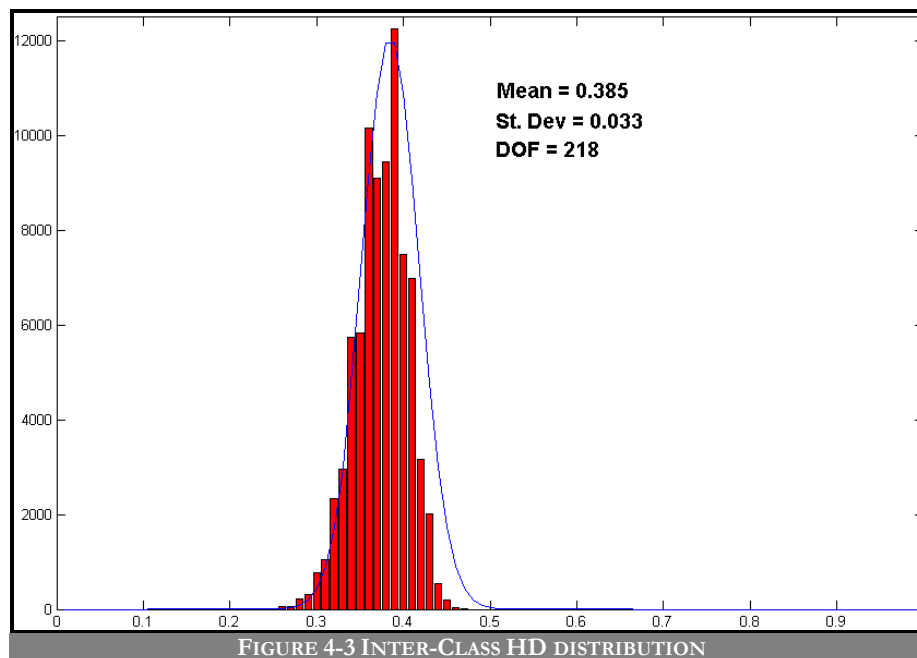
FIGURE 4-3 INTER-CLASS HD DISTRIBUTION

The HD distribution for intra-class distribution is shown in fig. 4.4.

FIGURE 4-4 INTRA-CLASS HD DISTRIBUTION
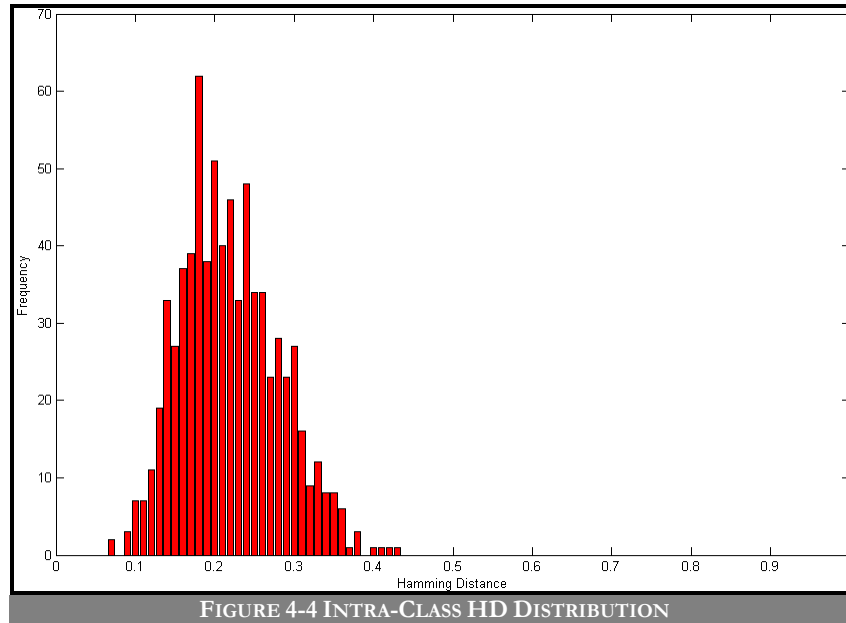
4.5 Discussion

As Figure 4.3 shows, the inter-class Hamming distance distribution. The statistical distribution in terms of FAR and FRR is listed in the following table:

HD Threshold	FAR	FRR
0.22	0.00	42.90
0.23	0.00	38.43
0.24	0.01	31.94
0.25	0.04	27.33
0.26	0.11	22.73
0.27	0.19	19.62
0.28	0.45	15.83
0.29	**0.82**	**12.72**
0.30	1.78	9.07
0.31	3.08	6.90
0.32	**5.98**	**5.68**
0.33	9.65	4.06
0.34	16.76	2.98
0.35	23.98	1.89
0.36	36.56	1.08
0.37	47.84	0.95
0.38	59.56	0.54
0.39	74.72	0.54
0.40	83.99	0.41
0.41	92.64	0.27
0.42	96.55	0.14
0.43	99.05	0.00
0.44	99.73	0.00
0.45	99.97	0.00
0.46	100.00	0.00

Distribution of FAR vs FRR is shown in the fig. 4.5

We can see a FAR of 0.01 up to a threshold value of 24, the reason for this much scoring of the a false template as a true one is that there is a huge number of ill conditioned images selected to take part into the testing of the system. In spite of all these situations we achieve fairly good results at a threshold of '.28' with FAR of just .82% and FRR of 12.72% and Equal Error Rate (EER) at '.32' of approximately '.57'. More over we get 218 degrees of freedom that are comparable to Daugman's system.

As shifting was introduced, so that intra-class templates were properly lined up, the mean inter-class Hamming distance value decreased as expected. The shifting also caused a reduction in the number of degrees of freedom, DOF. This reduction in DOF is an anomaly caused by a smaller standard deviation, which itself is caused by taking the lowest Hamming distance from 10 calculated values. This shows that, due to shifting, the distribution is not merely shifted towards the left, but the characteristics of the distribution are changed. Therefore the degrees of freedom formula is not very useful with shifting introduced, since it relies on the distribution approximating a binomial.

4.6 Individual Identification

The problem of recognizing the signature of a given iris as belonging to a particular individual, either after exhaustive search through a large database or just by comparison with a single authentication template, can be formulated within the framework of statistical decision theory. This framework also resolves the critical problem of assigning a confidence level to any such recognition decision. By this

approach we can convert the problem of pattern recognition into a much more expedient task, which is the execution of a simple test of statistical independence.

4.6.1 Neyman-Pearson Formalism

Yes/No recognition decisions have four possible outcomes: either a given pattern is, or is not, a true instance of the category in question; and in either case, the decision made by the algorithm may be either the correct one or the incorrect one. In the present application the four possible outcomes are termed Acceptance of Authentic (AA), Acceptance of Imposter (IA), Rejection of Authentic (AR), and Rejection of Imposter (IR). Obviously the first and fourth outcomes are desired, and the second and third outcomes are errors. The goal of the decision-making algorithm is to maximize the conditional probabilities of AA and IR, while minimizing the likelihoods of IA and AR. The pairwise trade-offs among the probabilities of these four outcomes can be manipulated in a way that reflects their associated costs and benefits in a particular application.

FIGURE 4-6 STATISTICAL DECISION THEORY: FORMALISM FOR DECISIONS UNDER UNCERTAINTY.
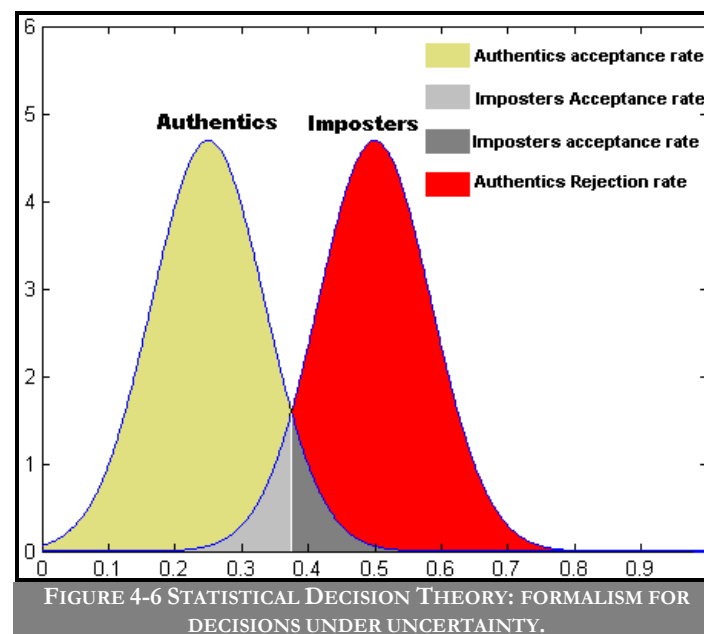
The Neyman-Pearson formalism for decision problems in which the prior probabilities are not known and the error costs are not fixed, but the posterior distributions are known, is summarized in Figure 4-6. A given measurement of the Hamming distance between two iris codes constitutes a point on the abscissa. This measurement is regarded as being a sample from one of two random processes (``Authentics'' or ``Imposters''), whose probability distributions have been arbitrarily

shown here as Gaussians with large overlap for purposes of illustration. The two distributions $P_{Au}(x)$, and $P_{Im}(x)$, specify respectively the probability density of a particular measured Hamming distance, x, arising from two comparisons of the same iris, or from two comparisons of different irises. Any measured Hamming distance smaller than a chosen decision criterion, as indicated by the dotted line in Figure 7, is judged to belong to the Authentics distribution, while any Hamming distance greater than this criterion is judged to belong to the Imposters distribution. The probabilities of the four possible outcomes AA, IA, AR, and IR are equal to the areas under the two probability density functions $P_{Au}(x)$ and $P_{Im}(x)$, on either side of the chosen decision criterion C:

$$P(AA) = \int_0^C P_{Au}(x)dx \qquad \text{Eq: 4-5}$$

$$P(AR) = \int_C^1 P_{Au}(x)dx \qquad \text{Eq: 4-6}$$

$$P(IA) = \int_0^C P_{Im}(x)dx \qquad \text{Eq: 4-7}$$

$$P(AA) = \int_C^1 P_{Im}(x)dx \qquad \text{Eq: 4-8}$$

These four probabilities are represented by the four shaded areas in Figure 7.

4.7 Strategies and Decidability

It is clear that the four probabilities separate into two pairs that must sum to unity, and two pairs are governed by inequalities:

$$P(AA) + P(AR) = 1 \qquad \text{Eq: 4-9}$$
$$P(IA) + P(IR) = 1 \qquad \text{Eq: 4-10}$$
$$P(AA) > P(IA) \qquad \text{Eq: 4-11}$$
$$P(IR) > P(AR) \qquad \text{Eq: 4-12}$$

It is also clear that the error rates, $P(AR)$ and $P(IA)$, could be minimized if the two Hamming distance distributions $P_{Au}(x)$, and $P_{Im}(x)$, had minimal overlap. Their overlap would be reduced if their two means were farther apart, or if their variances were smaller, of both. Of course, the two distributions in general will not be matched in form and variance, as was implied in Fig 4.6 for simplicity.

The overall "decidability" of the task of recognizing persons by their iris patterns is revealed by comparing the HD distributions for same versus for different irises. The distribution in Fig. 4.4 shows the HDs computed between different pairs of same-eye images. To the degree that one can confidently decide whether an observed sample belongs to the distribution in Fig. 4.3 or Fig. 4.4, iris recognition can be successfully performed. The "authentics" distribution for iris recognition (the similarity between different images of the same eye), depends very strongly upon the image acquisition conditions. However, the measured similarity for "imposters" is almost completely independent of imaging factors. Instead, it just reflects the combinatorics of Bernoulli trials, as bits from independent binary sources (the phase codes for different irises) are compared.

For two-choice decision tasks, such as biometric decision making, the "decidability" index d' is one measure of how well separated the two distributions are [5], since recognition errors would be caused by their overlap. If their two means are μ_1 and μ_2, and their two standard deviations are σ_1 and σ_2, then d' is defined as

$$d' = \frac{|\mu_1 - \mu_2|}{\sqrt{\frac{(\sigma_1^2 + \sigma_2^2)}{2}}}$$
Eq 4-1

This measure of decidability is independent of how liberal or conservative is the acceptance threshold used. Rather, by measuring separation, it reflects the degree to which any improvement in (say) the false match error rate must be paid for by a worsening of the failure-to-match error rate. The performance of any biometric technology can be calibrated by its score, among other metrics.

4.8 Liveness Detection

The operations described in chapter 2 for finding an iris also provide a good assessment of ``eyeness". The normally sharp boundary at the limbus between the iris and the (white) sclera generates a large positive circular edge; if a low value of cross correlation as described in section 2.3.1 or the voting score of the hough transform as described in section 2.1.3 is low, then it suggests either that no eye is present, or that it is largely obscured by eyelids, or that it is in poor focus or beyond resolution . In practice the automatic identifying system that has been built continues to grab image frames in rapid succession until several frames in sequence confirm that an eye is

apparently present, through large values being found by operations described as above.

A further test for evidence that a living eye is present exploits the fact that pupillary diameter relative to iris diameter in a normal eye is constantly changing, even under steady illumination [1]. Continuous involuntary oscillations in pupil size, termed hippus or pupillary unrest, arise from normal fluctuations in the activities of both the sympathetic and parasympathetic innervation of the iris sphincter muscle [1]. These changes in pupil diameter relative to iris diameter over a sequence of frames can be detected, in order to compute a ``hippus measure'' defined as the coefficient of variation (standard deviation divided by mean) for the fluctuating time series of these diameter ratios.

Chapter 5

Conclusion

5.1 Summary

This thesis has presented an iris recognition system, which was tested using two databases of grayscale eye images in order to verify the claimed performance of iris recognition technology.

Firstly, an automatic segmentation algorithm was presented, which would localize the iris region from an eye image and isolate eyelid. First of all a correlation operation was carried out to roughly estimate the pupil center, then a circular Hough transform was applied around that center to search for the pupil and then the iris.

After the successful detection of the two circles the iris area was normalized to a fixed size strip to compensate the factors like zooming and pupil dilation using Daugman's rubber sheet model. This normalized portion contains the occluded area, if present, in the form of a semicircle. So again circular Hough transform was employed for the detection of the occluded area of the eye.

The normalized image was subjected to the feature extraction algorithm, which was based on wavelets. Wavelet coefficients at different scales were selected and then quantized as 1 or 0 depending on their value to be positive or negative respectively. These 1's and 0's were used to form a binary code. For comparison between two eyes

hamming distance between the binary codes of the eyes was calculated and then the decision was made to according to a certain threshold of the distance after observing the distributions of the hamming distances. The code was shifted to right or left to compensate the head rotation.

5.2 Findings

Analysis of the iris recognition system reveals some interesting conclusions. The first and the foremost is that we can't just simply apply Hough transform to locate the desired objects, because it becomes so time consuming, takes lots of resources and does not give any real time response to a user. Hence to make the system practical, its necessary to adopt some optimization technique, that not only reduces the memory requirements but also the computations, while carrying out the same task.

On contrary to the suggestions of lots of literature that the occlusion should be detected before the normalization process, it was figured out that occlusion can be best modeled after normalization. This not only detects the occlusion perfectly but also reduced the computation time and detection process is not affected by the noise anymore.

After trying out different techniques of texture analysis for the feature extraction, it was found out that the wavelets performed the best among these techniques. The code generated gave only a little degradation in the presence of noise and the camera defocusing, hence making then system robust against the odds.

5.3 Suggestions for Future Work

The system designed was able to perform accurately, however there are still a number of issues which need to be addressed. The speed of the over all system is pretty good, it takes about 4-6 seconds to segment and match an eye. The system that has been developed has the potential to compete the commercial systems available in the market, but to achieve the performance level of these systems it should be ported to computer programming language like C or C++.

Another extension to the system would be to interface it to an iris acquisition camera. Now rather than having a fixed set of iris images from a database, a frame grabber can be used to capture a number of images, possibility improving the recognition rate.

An optimization whose feasibility could be examined with use of an acquisition camera would be the use of both eyes to improve the recognition rate. In this case,

two templates would be created for each individual, one for the left eye and one for the right eye. This configuration would only accept an individual if both eyes match to corresponding templates stored in the database. The recognition rates produced for this optimization would need to be balanced with the increased imaging difficultly, and inconvenience to the user.

To optimize the searching stage for a very huge database the eyes can be classified according to their colors. This would require colored pictures at the input stage; because of the unavailability of the colored images no such classifications could be done. This will dramatically reduce the matching time as matching will be performed with its class only.

REFERENCES

[1]   F.H. Adler, *Physiology of the Eye: Clinical Application* (fourth edition). London: The C.V. Mosby Company, 1965.

[2]   Ales Muron, Jaroslav Pospisil. Human Iris structure and its usages. In: Acta Univ. Palacki. Olomuc., Fac. Rer. Nat. (2000), Physica 39,87-95.

[3]   Christopher Coelle. The use and abuse of iris recognition.

[4]   J. Daugman. How iris recognition works. Proceedings of 2002 International Conference on Image Processing, Vol. 1, 2002.

[5]   J. Daugman. Biometric personal identification system based on iris analysis. United States Patent, Patent Number: 5,291,560, 1994.

[6]   J. Daugman. High confidence visual recognition of persons by a test of statistical independence. IEEE Transactions on Pattern Analysis and Machine Intelligence, Vol. 15, No. 11, 1993.

[7]   J.Daugman, "Statistical Richness of Visual Phase Information: Update on Recognizing Persons by Iris Patterns",International Journal of Computer Vision, Vol.45(1),pp.25-38, 2001.

[8]   J. Daugman. Biometric decision landscapes. Technical Report No. TR482, University of Cambridge Computer Laboratory, 2000.

[9]   R. Sanchez-Reillo and C. Sanchez-Avila, "Iris Recognition With Low Template Size", Proc. of International Conference on Audio and Video-based Biometric Person Authentication, pp. 324-329, 2001.

[10]   R. Wildes. Iris recognition: an emerging biometric technology. Proceedings of the IEEE, Vol. 85, No. 9, 1997.

[11]   R. Wildes, J. Asmuth, G. Green, S. Hsu, R. Kolczynski, J. Matey, S. McBride. A system for automated iris recognition. Proceedings IEEE Workshop on Applications of Computer Vision, Sarasota, FL, pp. 121-128, 1994.

[12]   Theodore A.Camus and Richard Wildes, "Reliable and Fast Eye Finding in Close-up Images", Proceedings of the IEEE International Conference on Pattern Recognition, 2002.

[13]   Rafael C. Gonzalez, Richard E. Woods. Digital Image Processing, 2nd edition. Pearson Education, 2002.

[14]   William K. Pratt. Digital Image Processing. John Wiley and Sons Inc. 2003.

[15]   Ballard D.H., Brown C.M. Computer vision. Prentice-Hall Inc. 1982.

[16]   Djemel Ziou, Salvatore Tabbone, "Edge Detection Techniques—An Overview", [10] C.Bouman, B.Liu, "Multi-resolution Segmentation of Textured Images", IEEE Trans. on Pattern Analysis and Machine Intelligence, Vol.13, pp.99-113, 1991.

[17]   Hough, P.V.C. Method and means for recognizing complexpatterns. U.S. Patent 3,069,654, Dec. 18, 1962.

[18] Richard O. Duda, Peter E. Hart. Use of Hough Transformation to detect lines and curves in pictures. Communications of the ACM, Vol:15, No. 1, Jan 1972.

[19] W. Kong, D. Zhang. Accurate iris segmentation based on novel reflection and eyelash detection model. Proceedings of 2001 International Symposium on Intelligent Multimedia, Video and Speech Processing, Hong Kong, 2001.

[20] Junzhou Huang, Yunhong Wang, Tieniu Tan, Jiali Cui. A new iris segmentation method for recognition. Proceedings of the 17th International Conference on Pattern Recognition (ICPR'04)

[21] Qi-Chuan Tian, Quan Pan, Yong-Mei Cheng, Quan-Xue Gao. Fast algorithm and application of Hough transform in iris segmentation. Proceedings of the Third International Conference on Machine Learning and Cybernatics, Shanghai, 26-29 August, 2004.

[22] C. H. Daouk, L. A. El-Esber, F. D. Kammoun and M. A. Al Alaoui. Iris Rcognition. IEEE ISSPIT 2002, Marrakesh - Page 558-562.

[23] D. Clausi, M. Ed Jernigan, "Designing Gabor filters for optimal texture separability," Pattern Recognition, vol. 33, pp. 1835-1849, 2000.

[24] T. P. Weldon, W. E. Higgins, D. F. Dunn, "Gabor filter design for multiple texture segmentation."

[25] Li Ma, Tieniu Tan, Yunhong Wang, Dexin Zhang, " Personal Identification Based on Iris Texture Analysis ", IEEE Transactions on Pattern Analysis and Machine Intelligence, VOL. 25, NO. 12, pp.1519-1533, 2003

[26] Li Ma, Tieniu Tan, Yunhong Wang, Dexin Zhang, " Efficient Iris Recognition by Characterizing Key Local Variations", accepted by IEEE Trans. on Image Processing.

[27] Li Ma, Y.Wang, T.Tan, "Iris Recognition Based on Multichannel Gabor Filters", Proc. of the Fifth Asian Conference on Computer Vision,Vol.I, pp.279-283, 2002

[28] Vincent Levesque. Texture Segmentation using Gabor Filters. Center For Intelligent Machines, McGill University December 6, 2000

[29] Li Ma, Y.Wang, T.Tan, "Iris Recognition Using Circular Symmetric Filters", Proceedings of the Sixteenth International Conference on Pattern Recognition, Vol.II, pp.414-417, 2002

[30] C. Tisse, L. Martin, L. Torres and M. Robert, "Person Identification Technique Using Human Iris Recognition" , Proc. of Vision Interface, pp.294-299, 2002.

[31] W. Boles, B. Boashash. A human identification technique using images of the iris and wavelet transform. IEEE Transactions on Signal Processing, Vol. 46, No. 4, 1998.

[32] C. Sanchez-Avila and R. Sanchez-Reillo, "Iris -based Biometric Recognition using Wavelet Transform", IEEE Aerospace and Electronic Systems Magazine, pp. 3-6, 2002.

[33] Jaemin Kim, Seongwon Cho And Jinsu Choi. Iris recognitin using wavelet features. Journal of VLSI Signal Processing 38, 147–156, 2004

[34] Y. Zhu, T. Tan, Y. Wang, " Biometric Personal Identification Based on Iris Patterns" , Inter. Conf. on Pattern Recognition (ICPR'2000), Vol.II, pp.805-808, 2000.

[35] P. Burt, E. Adelson. The laplacian pyramid as a compact image code. IEE Transactions on Communications, Vol. COM-31, No. 4, 1983.

[36] Chinese Academy of Sciences – Institute of Automation. Database of 756 Greyscale Eye Images. http://www.sinobiometrics.com Version 1.0, 2003.

[37] Multimedia University. Iris database http://pesona.mmu.edu.my/~ccteo/.

[38] UBIRIS database. http://iris.di.ubi.pt/

VITAE

The author, Azad Ali was born on May 20, 1980 in Sanghar district, Sindh, Pakistan. He got his early education from Sanghar. He did his matriculation from Govt: Boys School Sanghar in 1995. He completed his F.Sc. from Govt: degree college Sanghar in 1997.

He received degree of bachelor in Computer Systems Engineering from Mehran University of Engineering and Technology (MUET) Jamshoro Sindh in 2003. Pakistatn Institute of Engineering and Applied Sciences (PIEAS) awarded him fellowship in 2003 for M.Sc. System Engineering, at PIEAS, of which the current work is a part.

His research interests are Image Processing, Pattern Recognition, Computer Vision, embedded systems, Robotics and DSP.